

1 Revision #2

2 **Repeated, multiscale, magmatic erosion and recycling in an upper-crustal**  
3 **pluton: implications for magma chamber dynamics and magma volume**  
4 **estimates**

5

6 Scott Paterson<sup>1</sup>, Valbone Memeti<sup>2</sup>, Roland Mundil<sup>3</sup>, Jiří Žák<sup>4</sup>

7

8 <sup>1</sup> Department of Earth Sciences, University of Southern California, Los Angeles, CA 90089

9

10 <sup>2</sup> Department of Geological Sciences, California State University Fullerton, CA 92831

11

12 <sup>3</sup> Berkeley Geochronology Center, 2455 Ridge Road, Berkeley, CA 94709

13

14 <sup>4</sup> Institute of Geology and Paleontology, Faculty of Science Charles University, Albertov 6,  
15 Prague, 12843, Czech Republic

16

17 Abstract

18 The Tuolumne Intrusive Complex, an upper-crustal (7-11 kilometer emplacement  
19 depths), incrementally constructed (95-85 Ma growth history) plutonic complex  
20 (~1100 km<sup>2</sup>) preserves evidence from a number of datasets indicating the repeated,  
21 multi-scale, magmatic erosion of older units occurred and that some eroded  
22 material was recycled into younger magma batches. These include (1) map patterns  
23 of internal contacts (1000s kilometers) that show local hybrid units, truncations,  
24 and evidence of removal of older units by younger; (2) the presence of widespread  
25 xenolith and cognate inclusions (1000s), including “composite” inclusions; (3) the  
26 presence of widespread enclaves (millions), including “composite” enclaves, plus  
27 local enclave swarms that include xenoliths and cognate inclusions; (4) the presence  
28 of widespread schlieren-bound magmatic structures (>9000) showing evidence of  
29 local (meter-scale) truncations and erosion; (5) antecrystic zircons (billions) and

30 other antecrystic minerals from older units now residing in younger units; (6)  
31 whole rock geochemistry including major element, REE, and isotopic data; and (7)  
32 single mineral petrographic and geochemical studies indicating mixing of distinct  
33 populations of the same mineral. Synthesis of the above suggest that some erosion  
34 and mixing occurred at greater crustal depths but that 1000s of “erosion events” at  
35 the emplacement site resulted in removal of ~35-55% of the original plutonic  
36 material from the presently exposed surface with some (~25%?) being recycled into  
37 younger magmas and the remainder was either erupted or displaced downwards.  
38 The driving mechanisms for mixing/recycling are varied but likely include buoyancy  
39 driven intrusion of younger batches into older crystal mushes, collapse and  
40 avalanching along growing and oversteepened solidification fronts within active  
41 magma chambers (1 km<sup>2</sup> to >500 km<sup>2</sup> in size), and local convection in magma  
42 chambers driven by internal gradients (e.g., buoyancy, temperature, rheology).

43

44 Key words: Magmatic recycling, erosion, mixing, Sierra Nevada, solidification front  
45 erosion, Tuolumne Intrusive Complex,

46

## 47 **Introduction**

48 A broad discussion in the Earth Sciences community continues about the sorts of  
49 magmatic processes that take place within middle and upper crustal magma  
50 chambers (defined as interconnected regions of crystal-melt mixtures) before they  
51 crystallize into plutons (solidified intrusive bodies). Are these magma chambers  
52 small, ephemeral, and fairly static, in which little to no mingling, mixing, or

53 fractionation occur, or do large, longer-lived, dynamic magma chambers sometimes  
54 form in which extensive mixing, mingling and fractionation significantly change  
55 original magma source characteristics? A slight modification of this debate focuses  
56 on the degree to, and mechanisms by, which separate magma batches (e.g.,  
57 originally separate batches of crystal-melt mixtures) physically and chemically  
58 interact as they arrive in incrementally growing magma chambers or plutons  
59 (Michaut and Jaupart, 2006). As these new batches arrive preexisting material must  
60 be moved: there has been little discussion about how space is made for these  
61 younger batches as they move into the growing magma chambers or plutons. In the  
62 context of the previous questions, one can ask how younger batches displace older  
63 intrusive materials and whether some older material is recycled into arriving  
64 batches by mixing, physical incorporation or assimilation? The latter processes  
65 require some form of significant physical interaction in which younger batches,  
66 while still in a crystal mush state, can “erode” older materials and incorporate or  
67 “recycle” them into the arriving batch. Attempting to address many aspects of these  
68 debates draws attention to what sorts of processes occur along internal contacts  
69 either between separate batches (Bergantz, 2000; Žák and Paterson, 2005; Memeti  
70 et al, 2010) and/or along solidification fronts within magma chambers (Marsh, 1996,  
71 2006; Žák and Paterson, 2010).

72

73 Below we address the above questions by examining evidence for internal processes  
74 at scales ranging from ~100 kilometers to centimeters in the Tuolumne Intrusive  
75 Complex, or TIC (Fig. 1). This pluton has an ~10 m.y. history of growth and has been

76 used as an example of both an incrementally grown pluton in which little interaction  
77 has occurred between batches at the emplacement site, and thus source magma  
78 characteristics have been preserved (Coleman et al., 2004; Gray et al. 2008; Schöpa  
79 and Annen, 2013) and as a pluton where widespread magmatic mixing, mingling  
80 and fractionation resulted in significant compositional modification of source  
81 magmas at the emplacement level (Reid et al., 1993; Burgess and Miller, 2008; Žák  
82 and Paterson, 2010; Memeti et al., 2014).

83

#### 84 **Summary of previous work on Tuolumne Intrusive Complex**

85 The TIC is one of a number of ~1000 km<sup>2</sup> Cretaceous intrusive complexes that are  
86 exposed along the eastern crest of the Sierra Nevada and show a normal zonation  
87 from older, more mafic marginal phases to younger, more felsic, central phases (Fig.  
88 1; Bateman, 1992; Kistler and Fleck, 1994). These composite intrusions were  
89 emplaced at ~7–11 kilometer paleodepths (Ague and Brimhall, 1988; Memeti et al.,  
90 2009) during the Late Cretaceous (120–85 Ma) magmatic flare-up (Ducea, 2001;  
91 Paterson and Ducea, 2015). During construction of these plutons the arc was  
92 actively deforming during dextral transpression and vertical thickening (Tikoff and  
93 Greene, 1997; Tobisch et al., 2000; Cao et al., 2015). The TIC is a metaluminous,  
94 magnetite series intrusion that has a main body and four lobes extending outwards  
95 from the central body. The former consists of three major units nested into one  
96 another that become progressively younger and more SiO<sub>2</sub>-rich inwards and to the  
97 northeast (Memeti et al., 2010b, 2014). The outer 95–92 Ma Kuna Crest granodiorite  
98 (Fig. 1) is heterogeneous, ranging from mostly fine- to medium-grained

99 granodiorites and tonalites to local gabbroic, dioritic, and granitic compositions.  
100 Most Kuna Crest domains exhibit local sheeting along the outer margins of the  
101 batholith (Memeti et al., 2014) and moderately intense magmatic and local  
102 subsolidus fabrics. The 92–88 Ma Half Dome Granodiorite (Fig. 1) is subdivided into  
103 an outer equigranular unit characterized by conspicuous euhedral hornblende ( $\leq 2$   
104 centimeter lengths), biotite books and titanite, and the inner porphyritic unit, which  
105 contains K-feldspar phenocrysts up to  $\sim 3$  centimeters long and fewer mafic  
106 minerals (Bateman and Chappell, 1979). The 88–85 Ma Cathedral Peak unit (Fig. 1)  
107 is mainly composed of medium-grained granodiorite with up to 12-centimeter long  
108 K-feldspar phenocrysts and 1 centimeter quartz aggregates (Bateman and Chappell,  
109 1979). The Cathedral Peak is a granite in places, especially in the northern Cathedral  
110 Peak lobe (Memeti, 2009).

111         Each of the four lobes compositionally consists of one of the main units in the  
112 central body, thus forming two southern lobes, one extending out from the  
113 porphyritic Half Dome unit and one from the Kuna Crest unit, and two northern  
114 lobes, one extending out from the equigranular Half Dome unit and the other  
115 forming the NE end of the Cathedral Peak (Fig. 1). Each lobe shows internal zoning  
116 from more mafic margins to more felsic centers and inward younging U/Pb zircon  
117 ages (e.g., Memeti et al., 2010). All of these units, both in the main body and in the  
118 four lobes, locally contain regions of late leucogranites with stock-like, sheet-like or  
119 cross-cutting dike-like shapes, the largest of which is the ca. 87.5 Ma Johnson  
120 Granite Porphyry (Bateman and Chappell, 1979; Bracciali et al., 2008).

121

122 *Geochemistry*: Bateman and Chappell (1979) used major- and trace element  
123 compositions to argue for closed-system fractional crystallization to explain the  
124 roughly concentric compositional zoning in the TIC. A subsequent Nd-Sr isotope  
125 study by Kistler et al. (1986) revealed differing isotopic values for different TIC units  
126 that were better explained as mixtures of mantle-derived basaltic and crustal  
127 granitic magmas, with the latter magmas increasing in younger units. Gray (2003)  
128 and Gray et al. (2008) argued that major- and trace-element variations in the TIC are  
129 decoupled from each other and that their lack of any uniform spatial pattern can be  
130 best explained by incremental emplacement through diking, implying that any  
131 geochemical variability is due to source heterogeneity. However, Memeti et al.  
132 (2009, 2014) challenged this conclusion and instead argued that major- and trace-  
133 element variations define separate but overlapping mixing trends for the different  
134 TIC units. Coleman et al. (2004) used a geochronologic database to argue that little  
135 fractionation or mixing occurred at the emplacement site (see also, Coleman, 2005;  
136 Gray, 2003; Gray et al., 2008). Memeti and colleagues examined the peripheral 10-  
137 40 km<sup>2</sup> magmatic lobes of the TIC to evaluate the crystallization history, causes of  
138 normal zoning (older, mafic marginal units to younger, felsic interiors) preserved in  
139 each lobe (Memeti, 2009; Memeti et al., 2010). Geochemical histories exist between  
140 lobes with the southern HD lobe dominated by fractionation (Economos et al., 2010)  
141 and others typically preserving more complicated histories of amalgamation of  
142 batches, fractionation, and mixing (Memeti et al., 2010; 2014; Barnes et al., 2016).  
143  
144 Several authors have examined the geochemistry of schlieren-bound magmatic

145 structures within the TIC (Reid et al., 1993; Solgadi and Sawyer, 2007; Burgess and  
146 Miller, 2008; Paterson et al., 2008; Paterson, 2009; Žák et al., 2009). These studies  
147 are in general agreement and indicate that: (1) the sharp bases of schlieren show a  
148 modal increase in biotite and hornblende and an unusually high increase in  
149 accessory minerals including zircon, sphene, apatite, rare allanite, magnetite and  
150 other oxides and thus are cumulates; (2) that the composition of the schlieren are  
151 dramatically different than host magma compositions, do not follow the trends seen  
152 in the main units, have high REE enrichments reaching 800-1000 times chondritic  
153 values for LREE's, and are compatible with depletion in  $\text{Al}_2\text{O}_3$ ,  $\text{Na}_2\text{O}$  and enrichment  
154 in Rb, MgO, CaO,  $\text{K}_2\text{O}$ ,  $\text{TiO}_2$ ,  $\text{P}_2\text{O}_5$ , Zr, Y, La, and Ce relative to nearby plutonic  
155 material; and (3) that the origin of schlieren cannot be due to a simple  
156 accumulation of crystals during fractional crystallization but require  
157 mixing/mingling and/or erosion and recycling of material from older batches (Ardill  
158 et al., 2015). Solgadi and Sawyer (2007) particularly noted that microprobe analyses  
159 of hornblendes from these schlieren define three distinct populations that  
160 compositionally match those seen in the three main units (KC, HD, CP) of the TIC.  
161 They concluded that mechanical erosion, mixing of crystals, and redeposition played  
162 a dominant role in schlieren formation.

163

164 Wallace and Bergantz (2002), Krause et al. (2009, 2010), Memeti et al. (2009, 2013,  
165 2014), and Barnes et al. (2016) have recently focused on mineral-scale geochemical  
166 studies and concluded that the geochemical zonation pattern of K-feldspars,  
167 plagioclase, hornblende, biotite, and titanite show varied internal patterns that often

168 require mixing of disparate crystal populations. Thus a large, published geochemical  
169 dataset, including both whole rock and mineral-scale major element, REE, and  
170 isotopic data support the conclusion that crystal-crystal and crystal-melt mixing,  
171 from hand sample to > 10 kilometer scales, is widespread in the TIC.

172

173 *Geochronology of the TIC:* Early studies of the TIC using U/Pb, Rb-Sr, K-Ar, and  
174  $^{40}\text{Ar}/^{39}\text{Ar}$  techniques recognized that its assembly took millions of years (Stern et al.,  
175 1981; Fleck and Kistler, 1994; Kistler and Fleck, 1994). A more recent study carried  
176 out by Coleman et al. (2004) determined an ~9 m.y. construction history for the TIC  
177 and concluded that the TIC in general, and the Half Dome pluton in particular, must  
178 have been formed from multiple small batches of magma, perhaps as a series of  
179 sheets or dikes. Furthermore, they argued that convecting, fractionating and mixing  
180 magma chambers were rare or absent and as a consequence, that the geochemical  
181 trends observed in the TIC must be inherited from the magma source characteristics  
182 rather than modified by in situ processes. However, the Coleman et al. (2004) study  
183 used multi-crystal analyses of zircon populations that have been shown to be  
184 particularly prone to unrecognized Pb loss and age-averaging effects of analyzing  
185 mixed autocrysts, antecrysts and xenocrysts (Mundil et al., 2001; Miller et al. 2007;  
186 Memeti et al., 2014).

187

188 It is now well established in a number of plutonic and volcanic systems, including  
189 the TIC, that zircon populations often contain mixed zircon populations (Fig. 2a)  
190 including xenocrysts (inherited from older host rocks or melt source regions),



191 antecrysts (recycled from earlier batches of magma), and autocrysts (grown in final  
192 melts)(e.g., Hildreth, 2004; Bacon and Lowenstern, 2005; Miller et al., 2007). In  
193 such mixed populations the youngest zircon ages (Fig. 2a) probably best represent  
194 the time when zircon crystallization ended if Pb loss can be entirely excluded (Irmis  
195 et al., 2011). Because zircon crystallizes over a fairly narrow temperature range in  
196 calc-alkaline magmas as a function of Zr saturation, zircon ages cannot be equated to  
197 an emplacement or arrival age of magma batches but instead are a better estimate  
198 of late crystallization. Memeti et al. (2010) presented new U-Pb, CA-ID-TIMS, single-  
199 crystal analyses on 224 individual zircons or zircon fragments from 26 samples  
200 across the TIC. Figure 1 displays these new TIC ages determined from the youngest  
201 autocrystic zircons (see Ickert and Mundil, 2015 for calculation methods). The new  
202 data show a general inwards and northerly younging pattern in the main pluton and  
203 local inward younging patterns of different ages in the 4 lobes extending outward  
204 from the main pluton (Memeti et al., 2014).

205

206 Matzel et al. (2006b) and Memeti et al. (2014) also discuss new  $^{40}\text{Ar}/^{39}\text{Ar}$  ages from  
207 the TIC and adjacent older units. Samples collected along two SW-NE corridors  
208 across the TIC, in the lobes, and in local host units were used to separate two  
209 different biotite and hornblende grain-size fractions (800–900  $\mu\text{m}$  and 150– 180  
210  $\mu\text{m}$ ).  $^{40}\text{Ar}/^{39}\text{Ar}$  step heating for large single crystals (hornblende and biotite) as well  
211 as total fusion experiments (small crystals) were performed on these populations  
212 from each sample (Fig. 2b). Besides establishing a general subsolidus cooling  
213 pattern in the TIC and nearby host rocks that roughly mimics the zircon age pattern,

214 these biotite ages show that cooling from the margin to central parts of the TIC was  
215 non-linear and that large parts of the TIC show similar cooling ages (Fig. 2b).

216

217 In regard to the theme of the present paper, there are several important aspects of  
218 the new geochronologic data: (1) zircon antecrysts are rare in the outer/older Kuna  
219 Crest units and increase in abundance in the inner units (Fig. 2a). Memeti et al.  
220 (2014) concluded that this result occurred from mixing or recycling of zircons from  
221 older units into younger units; (2) a comparison of local gradients in zircon ages  
222 across mapped internal contacts indicate that monotonous inward younging  
223 (argued for by Coleman et al., 2004) is not the general pattern and instead several  
224 “kinks” with gentle slopes at ~94 Ma, 90 Ma, and particularly at ~88-87 Ma, are  
225 spatially associated with mapped internal contacts (Memeti et al., 2014). These  
226 observations suggest that there are both age jumps across internal contacts and that  
227 at certain times simultaneous zircon crystallization occurred over broad areas in the  
228 TIC, indicating the presence of larger magma chambers; (3) zircons with ages of  
229 these broader regions occur as antecrysts in younger units suggesting that the  
230 original extent of older units (e.g., Kuna Crest or Half Dome granodiorites) were  
231 significantly larger and subsequently displaced and partly assimilated during  
232 intrusion of the younger units; (4) autocrystic zircon ages typically show an age  
233 dispersion (greater than errors) along concordia that extend from a few hundred  
234 thousand to over 1 million years (Fig. 2a), raising the possibility that melt from  
235 which these zircons grew also existed in the TIC for at least these durations; (5) the  
236 biotite cooling ages also show broad regions with similar cooling ages (Fig. 2b),

237 suggesting that either larger magma batches arrived in the growing pluton or if  
238 these regions grew incrementally, they did so rapidly and formed large magma  
239 chamber(s) that shared similar autocrystic zircon growth and biotite cooling  
240 histories.

241

242 We suggest that the geochronology supports the following hypotheses: (1) batch  
243 arrival times remain poorly constrained but must be slightly before the ages in  
244 Figure 1; (2) batch sizes are variable and remain poorly constrained; (3) zircon and  
245 biotite ages indicate that at least three times during construction of the TIC fairly  
246 large magma chambers existed in the main batholith and smaller ones in the lobes.  
247 (4) Durations of these magma chambers could have easily ranged from 0.5 (lobes)  
248 to 1.5 m.y. (main pluton) given the spread of autocrystic zircon ages plus any  
249 additional melt residence time before zircon growth. This conclusion is supported  
250 by thermal models of the TIC (Paterson et al. 2011), by the transfer of latent heat of  
251 crystallization to the melt (e.g., Michaut and Jaupart, 2006) and by the recognition  
252 that magmas are “thermally insulating” as thermal diffusivity and conductivity are  
253 drastically decreased in magma mushes at higher temperatures (Whittington et al.,  
254 2009; Nabelek et al., 2012).

255

## 256 **INTERNAL CONTACTS**

257 Internal contacts provide information either about magma chamber or pluton  
258 construction during incremental growth or about internal magma chamber  
259 processes that may be somewhat independent of pluton growth (e.g., Pitcher and

260 Berger, 1972; Hardee, 1982; Hutton, 1982, 1992; Lagarde et al., 1990; Paterson and  
261 Vernon, 1995; McNulty et al., 1996; Vignerresse and Bouchez, 1997; Paterson and  
262 Miller, 1998; Wiebe and Collins, 1998; Johnson et al., 1999; Paterson et al., 2011).  
263 Internal contacts in granitoids have variable characteristics such as: (1) sharp or  
264 gradational; (2) defined by distinct compositions and/or distinct microstructures;  
265 (3) along-strike lengths that range from centimeters to kilometers, and (4) the  
266 presence or absence of magmatic structures (e.g., host rock rafts, troughs, enclaves,  
267 and schlieren) or objects (e.g., enclaves, stoped blocks, rafts) concentrated along  
268 them. Contacts between the TIC units vary from knife sharp to gradational over  
269 hundreds of meters (Bateman and Chappell, 1979; Bateman, 1992; Žák and  
270 Paterson, 2005). The different types of internal contacts may form by (1) the  
271 addition of new magma batches into a magma chamber, (2) localized flow of magma  
272 with different viscosities within an existing magma chamber, and (3) processes  
273 during crystallization, such as crystal-liquid fractionation. The latter two processes  
274 imply that internal contacts may not necessarily imply the arrival of multiple  
275 magma batches during growth of a pluton.

276

277 Figure 1 displays the position and general nature of the main internal contacts in the  
278 TIC. Several patterns have emerged. First, these contacts can be followed for  
279 distances from 1 to 100 kilometers. Second, a single contact will often vary in  
280 character from sharp to gradational along strike sometimes over scales of 100s of  
281 meters. Even so, certain contacts tend to typically be sharp or gradational no matter  
282 which older units are juxtaposed across the contact. For example, the outer

283 Cathedral Peak contact is commonly quite sharp against either pre-TIC host rocks or  
284 the porphyritic Half Dome unit. Some late leucogranites also have sharp contacts  
285 against older units. However, the contact between the Kuna Crest-equigranular Half  
286 Dome units is more often gradational or has preserved hybrid units along it (Fig. 1).  
287 Although the previously discussed zircon geochronology was not collected with the  
288 target of evaluating age variations across internal contacts, both the ages reported  
289 by Coleman et al. (2004) and by Memeti et al. (2010) are suggestive of a relationship  
290 between contact sharpness and an increasing magnitude of age jumps across the  
291 contacts.

292

293 A number of maps of internal contacts, constructed at 1:10,000 scale, have been  
294 completed in the TIC (Fig. 1), and four examples (Fig. 3, 4, 5, 6) indicate the variable  
295 nature of these contacts, including the presence of “hybrid” magmatic zones locally  
296 formed between units and the presence of a number of truncations of older units by  
297 younger.

298

299 *Glen Aulin*: The ~102 Ma El Capitan granite forms a prominent eastward protrusion  
300 that TIC units wrap around near the western margin of the TIC. Here the outermost  
301 units of the TIC tend to broadly follow the border of this protrusion (Fig. 3). In  
302 detail some important map patterns exist. First small pendants and rafts of  
303 metamorphic host rock, all considered to be pieces of the former Snow Lake block  
304 consisting of Paleozoic passive margin assemblages (e.g., Memeti et al., 2010a),  
305 occur near or at the external contact between the El Capitan and TIC. The most

306 remarkable case is a 5 centimeter to meter wide strip of metamorphic rock  
307 immediately at the contact between the two plutons north of Glen Aulin that, in spite  
308 of its thin width, is still preserved. Other host rock occurs as blocks or rafts within  
309 the two plutons. Here the outermost unit of the TIC, excluding local mafic cumulates,  
310 is called the Glen Aulin tonalite, which is considered to be part of the Kuna Crest unit.  
311 The next major unit is the equigranular Half Dome granodiorite with its prominent  
312 euhedral hornblendes and sphene. Locally a hybrid unit with shared Kuna and Half  
313 Dome characteristics occurs between the two units (Fig. 3). Along strike the contact  
314 is sharp and no hybrid unit exists. The equigranular Half Dome granodiorite changes  
315 gradually inwards into the porphyritic Half Dome granodiorite, which is also  
316 discontinuous along strike (Fig. 3). The most extensive, innermost and youngest unit  
317 mapped in this area is the Cathedral Peak granodiorite with its large K-feldspar  
318 megacrysts and more abundant biotite than hornblende. Close inspection shows  
319 that the Cathedral Peak contact is typically sharp and in places cuts across both Half  
320 Dome units and directly intrudes the Kuna Crest. Except for the Cathedral Peak  
321 granodiorite, all other units are surprisingly thin in this area compared to their  
322 exposed thicknesses elsewhere in the TIC.

323

324 *Kuna Crest units in Upper Lyell Canyon:* Two NW-striking, steeply dipping tonalite to  
325 granodiorite Kuna Crest units have been mapped along the SW margin of this lobe  
326 by Memeti et al. (2010). These units are sharply truncated (near Ireland Lake on Fig.  
327 4) by an ~east-west striking, steeply dipping, younger Kuna Crest granodiorite unit  
328 and an east-west striking fairly homogenized, Kuna Crest-Half Dome hybrid unit

329 sharing field and geochemical characteristics of both of these units (Fig. 4). The  
330 detailed characteristics and geochemistry of intrusive units in this lobe are  
331 presented by Memeti et al. (2010, 2014).

332

333 *Fletcher Peak area:* Žák and Paterson (2005) examined the geology in the Fletcher  
334 Peak area near the southern end of the TIC (Fig. 1, 5). Here the ~97 Ma Ireland Lake  
335 granite intrudes older metavolcanic units and together these two units make up the  
336 host rock that the TIC intruded. The Kuna Crest granodiorite intrudes these host  
337 rocks, contains host rock blocks and rafts in it, and forms an east-west striking,  
338 steeply dipping intrusive unit that strikes towards the east-west Kuna Crest unit in  
339 Figure 4. The western end of this east-west Kuna Crest unit is truncated by a  
340 complex mingling zone consisting of hybrid units, local sheeting, and a variety of  
341 magmatic structures. The porphyritic Half Dome unit intrudes this mingling zone  
342 along a sharp contact that truncates structures within the mingling zone. No  
343 equigranular Half Dome unit is preserved here except in local areas within the  
344 mingling zone or within magmatic structures in this zone. Finally, the Cathedral  
345 Peak unit intrudes the inner part of the porphyritic Half Dome unit along another  
346 sharp contact.

347

348 *Sawmill Canyon area:* Paterson et al. (2008; 2014) discuss complex cross-cutting  
349 intrusive relationships in the Sawmill Canyon area along the eastern margin of the  
350 TIC (Fig. 1, 6). These authors established that the northward striking and steeply  
351 dipping outer and older (~94-95 Ma) Kuna Crest unit and adjacent inner and

352 younger (~92-88 Ma) equigranular Half Dome granodiorite are sharply truncated,  
353 at the centimeter to meter scale, by an east-west striking, complicated sheeted and  
354 mingled zone dominated by a variety of magmatic structures. This sheeted zone  
355 swings to the NNW along the NNW striking eastern margin of the TIC (Fig. 6) and  
356 then is eventually truncated by the younger (~88 Ma) Cathedral Peak granodiorite.  
357 North of the Sawmill Canyon area, the Kuna Crest unit is completely absent. Only  
358 two blocks, one large (100s of meters) and one small (several meters) of Half Dome  
359 granodiorite have been found north of the Sawmill Canyon area, and are now largely  
360 surrounded by Cathedral Peak granodiorite (Fig. 6a). Field mapping and  
361 geochemical studies from within the “sheeted zone” (Paterson et al., 2008) indicate  
362 that much of the material is made up of porphyritic Half Dome magma, but that a  
363 complete mingling of Kuna Crest, Half Dome, and Cathedral Peak phases (both solid  
364 pieces and crystal mush mingled phases) make up this zone. Smaller versions of  
365 these sheeted zones crop out immediately south of the Sawmill Canyon area along  
366 what are interpreted to be east-west striking cracks that were filled by pulses of  
367 magma (Paterson et al., 2008). The main Sawmill Canyon sheeted zone is  
368 interpreted to have formed along one of these cracks across which the northern  
369 Kuna Crest and Half Dome phases were eventually removed.

370

371 The map patterns presented above provide examples of two important concepts.  
372 The first is that hybrid magmatic zones bordered by gradational contacts sometimes  
373 form in between the main TIC units. These hybrid units range from fairly  
374 homogenized zones with mineralogical characteristics of the two adjacent units, to



375 irregular, heterogeneous (less homogenized) zones with different parts sharing  
376 characteristics of one of the two adjacent rock types. This suggests that some degree  
377 of mixing or mingling between adjacent units occurred and required at least  
378 sufficient interconnected melt in both units. Sometimes these “hybrid” zones can be  
379 very complex (e.g., Fletcher Peak and Sawmill Canyon) with sheeting and a variety  
380 of compositionally defined magmatic structures suggesting that they were active  
381 zones of magma pulsing, mixing, mingling, and local convection.

382

383 The second concept is that the map patterns show examples of repeated truncations,  
384 and thus implied removal or erosion of older by younger intrusive units along these  
385 contacts. These truncations, sometimes regional in extent, can be viewed at the  
386 meter to centimeter scale and in cases shown to truncate local compositionally  
387 defined contacts, or compositionally defined magmatic structures, and in rare cases  
388 even large phenocrysts. The truncation of these objects suggests that complex  
389 brittle-ductile behavior occurred during removal or “erosion” of older materials  
390 (typically crystal-rich mushes) during intrusion of younger magma batches.

391

### 392 **Outcrop-scale examples of erosion/recycling**

393 At 1 to 10 meter scales three features support repeated erosion/recycling: (1)  
394 “composite” xenoliths of host rocks or cognate inclusions of older parts of the TIC  
395 now present as blocks in younger plutonic phases; (2) widespread and fairly evenly  
396 distributed mafic enclaves and local enclave swarms with xenoliths; and (3) a  
397 variety of compositionally defined magmatic structures that are sharply truncated

398 by younger magma batches implying erosion of older crystal mushes and removal or  
399 recycling of these mushes. We present examples of these below.

400

401 Xenoliths (solid objects of material foreign to the TIC) and cognate inclusions (fairly  
402 coherent blocks of solid material or crystal mushes from an earlier part of the TIC)  
403 occur in all units within the TIC (Fig. 7, 8, 9, 10). The most exciting examples include  
404 “composite” cases where an older object is surrounded by an older plutonic phase  
405 and in turn both are surrounded by younger plutonic phase. Fig. 7 shows a number  
406 of examples from the Kuna Crest unit. Figure 7a shows Paleozoic metasedimentary  
407 stoped blocks, 7b older plutonic, volcanic and mafic enclaves in a large mafic enclave  
408 now in a Kuna Crest matrix, 7c, 7d, and 7e depict “composite” blocks of Jurassic  
409 volcanic blocks (7c, 7e) and calc-silicate metasediments (7d), respectively,  
410 surrounded by mafic Kuna Crest tonalite in more felsic Kuna Crest granodiorite.  
411 Figure 7f displays numerous cognate inclusions and mafic enclaves and rare  
412 xenoliths in a hybrid Kuna Crest granodiorite. Note that in all of the above examples,  
413 the compositional heterogeneity over short distances and variable structural  
414 orientations between nearby blocks support that these blocks have moved  
415 significantly from their site of origin accumulated in the present location.

416

417 Figure 8 shows similar examples residing in a matrix of Half Dome granodiorite.  
418 Figures 8a and 8b show metavolcanic and metasedimentary xenoliths in the Half  
419 Dome granodiorite. Figures 8c and 8d show composite cognate inclusions of former  
420 enclave swarms with local xenoliths that are attached to a matrix of Kuna Crest

421 granodiorite and now reside together in equigranular Half Dome granodiorite. Note  
422 the sharp boundaries defining the rectangular shape of the blocks that cut and  
423 truncate individual enclaves indicating that a former more elongate enclave swarm  
424 (e.g., Tobisch et al., 1997) was broken apart into rectangular pieces, presumably  
425 during movement of Kuna Crest magma, and subsequently was incorporated into  
426 Half Dome magma. Figure 8e displays a composite block of volcanic pieces locally  
427 attached to and intruded by Kuna Crest magma now surrounded by a Half Dome  
428 granodiorite matrix. Figure 8f shows a collection of xenoliths, a large cognate  
429 inclusion of layered plutonic rock and numerous enclaves near the Kuna Crest – Half  
430 Dome contact.

431

432 Figure 9 shows inclusions residing in the Cathedral Peak granodiorite. Figure 9a  
433 shows a folded metavolcanic xenolith, 9b a cognate inclusion of Half Dome  
434 granodiorite, 9c a layered cognate inclusion of porphyritic Half Dome magma and 9d  
435 a composite inclusion of layered plutonic rock rimmed by Half Dome plutonic  
436 material in the Cathedral Peak granodiorite. Figure 9e shows a schlieren-bound tube  
437 sharply truncated by Cathedral Peak magma and 9f shows a composite inclusion  
438 with a small piece of layered plutonic rock (white arrow) in a matrix of layered Half  
439 Dome granodiorite (HD), now entirely surrounded by Cathedral Peak granodiorite.

440

441 Figure 10 shows various pieces of the Cathedral Peak granodiorite in the Johnson  
442 granite. Figure 10a shows Cathedral Peak K-feldspar megacrystic antecrysts, 10b an  
443 angular piece of Cathedral Peak granodiorite, and Figure 10c and 10d rounded

444 (presumably by partial melting) pieces of Cathedral Peak, each with one large K-  
445 feldspar megacryst in a medium-grained Cathedral Peak granodiorite matrix, in the  
446 fine grained Johnson granite.

447

448 Figures 7-10 document that pieces of host rock or older parts of the TIC have been  
449 broken, moved, and are now in younger parts of the intrusive complex and thus  
450 provide direct evidence of “recycling” of material into new magma batches. The  
451 composite examples are particularly exciting since they require at least two  
452 “recycling events” to form. There is no evidence that any of these inclusions are  
453 traditional rafts that haven’t moved from their site of origin. Instead all are now  
454 located at some distance from the nearest likely sources, show along-strike changes  
455 in rock type with nearby blocks, and typically show internal structures that are  
456 rotated from both regional structural patterns and nearby blocks. If one argues that  
457 the blocks haven’t moved very far, the presence of older magmatic phases of the TIC  
458 in regions where only a younger phase is now preserved indicates that the older  
459 phases were originally more extensive and have since been removed and/or  
460 displaced out of the present plane of exposure.

461

462 Another feature in the TIC that deserves careful consideration in regards to  
463 mixing/recycling of magmas are the characteristics of enclaves and enclave swarms  
464 (Fig. 11). A great deal of attention was paid to enclaves in past Sierran studies (e.g.  
465 Pabst, 1928; Frost and Mahood, 1987; Barbarin, 1990, 2005; Tobisch et al., 1997)  
466 but little work has been published on them recently. Barbarin (2005) noted that

467 both mafic dikes and mafic enclaves in central Sierran plutons exhibit a bulk  
468 compositional diversity but with broadly overlapping major, trace element and  
469 isotopic compositions and argued that both were produced by the mixing of the  
470 same two components in different proportions. Based on enclave microstructures  
471 and geochemistry, Barbarin (2005) concluded that a few enclaves formed from early  
472 cumulates at depth, whereas most formed by disruption and mingling/mixing of  
473 mafic dikes (e.g., Frost and Mahood, 1987) and some by disruption of schlieren at  
474 the level of emplacement. Their initial formation was followed by the sequential  
475 mixing and mingling during widespread dispersion, followed locally by collection  
476 processes to form enclave swarms (see also Tobisch et al., 1997). Barbarin (2005)  
477 also noted less common “composite enclaves” that consist of either host rock  
478 xenoliths enclosed in a mafic enclave, or one style of mafic enclave enclosed in  
479 another, both now residing in a younger more felsic granitic matrix.

480

481 Mafic microgranitoid enclaves are widespread in the TIC and occur in all of the three  
482 main units, although they are rare in the late leucogranites (Fig. 11). We also find  
483 less common synmagmatic mafic dikes (Fig. 11a) in various degrees of  
484 disaggregation (Fig. 11b) and enclave formation (Memeti and Paterson, 2007). Most  
485 TIC enclaves form roughly elliptical shapes and are remarkably evenly spaced (Fig.  
486 11c). Local enclave swarms are fairly common in the TIC (Fig. 11d). These enclave  
487 swarms often include not only enclaves but cognate inclusions and host rock  
488 xenoliths supporting the interpretation that they are physical accumulations of  
489 formerly dispersed objects in the magma chamber. Composite enclaves locally occur

490 (Fig. 11e) and some rectangular cognate blocks consist of former enclave swarms  
491 (Fig. 8c, 8d, 11f). These observations thus imply that many enclaves formed from  
492 disaggregated dikes, followed by dispersion in a magma chamber (by convection),  
493 followed by some form of local flow sorting resulting in accumulations of not only  
494 enclaves but previously formed xenoliths and cognate inclusions. Finally sometimes  
495 the enclave swarms are reintruded and broken into new cognate blocks.

496

497 Reid et al. (1993), Burgess and Miller (2008), Solgadi and Sawyer (2008), Paterson  
498 (2009), and Hodge et al. (2012) described a variety of compositionally defined  
499 magmatic structures in the TIC. For purposes of this paper, we focus on schlieren-  
500 defined tubes and troughs that repeatedly show sharp truncations of older parts of  
501 these structures and sometimes show evidence of reintrusion and recycling of the  
502 broken pieces into younger magmatic phases. Fig. 12 shows examples of these  
503 structures, which occur in all units of the TIC although they are most common in the  
504 Cathedral Peak and Half Dome granodiorites. Figures 12a and 12b show mafic  
505 schlieren defining two sets of magmatic troughs showing examples of sharp  
506 truncations of older schlieren layers. These truncations are visible at the centimeter  
507 scale and sharply cut across both mafic and felsic layers as well as subparallel  
508 magmatic mineral foliations with no deflection of the older layers. A new magmatic  
509 foliation is subparallel to the new, cross-cutting schlieren layer. Figure 12c shows a  
510 package of mafic-felsic schlieren layers of Half Dome granodiorite, defined by  
511 grading in proportions of mafic minerals, that were sharply truncated by younger  
512 batches of magma. None of the layers show any deflection or gradation into the

513 younger plutonic material. Figure 12d shows schlieren in porphyritic Half Dome  
514 granodiorite that are sharply truncated by younger schlieren layers. Figure 12e  
515 shows an example of a “bifurcated” schlieren-bound migrating tube(s), with  
516 repeated truncations of older tube margins by younger, now surrounded and locally  
517 reintruded by Cathedral Peak granodiorite. These structures have magmatic fabrics  
518 parallel to the bases of the mafic layers that are overprinted by magmatic fabrics  
519 that are continuous from the surrounding Cathedral Peak granodiorite into the  
520 magmatic structures (e.g. Paterson, 2009). Figure 12f is an example in Cathedral  
521 Peak granodiorite of planar schlieren and subparallel magmatic foliation truncated  
522 by and presumably removed during the formation of a schlieren bound trough in  
523 which a new schlieren-parallel foliation is formed.

524

525 Studies of the compositions of these structures (e.g., Reid et al., 1993; Solgadi and  
526 Sawyer, 2007; Burgess and Miller, 2008; Paterson et al., 2008; Žák et al., 2009;  
527 Paterson, 2009) are in general agreement and indicate that: (1) the sharp bases of  
528 schlieren are marked by an abruptly higher concentration of biotite and hornblende  
529 and an unusually high concentration of accessory minerals including zircon, sphene,  
530 apatite, rare allanite, magnetite and other oxides, and thus are cumulates; (2) the  
531 compositions of the schlieren are dramatically different than host magma  
532 compositions, do not follow the trends seen in the main units, have high REE  
533 abundances reaching 800-1000 times chondrites for LREE's, lower abundances in  
534  $\text{Al}_2\text{O}_3$ ,  $\text{Na}_2\text{O}_3$  and higher abundances in Rb, MgO, CaO,  $\text{K}_2\text{O}$ ,  $\text{TiO}_2$ ,  $\text{P}_2\text{O}_5$ , Zr, Y, La, and  
535 Ce; and (3) that the origin of the schlieren cannot be simple accumulations of the

536 mafic and accessory minerals from a single magma, but instead require two or more  
537 sources for these minerals. Solgadi and Sawyer (2007) particularly noted that  
538 compositions of hornblendes from schlieren in the Sawmill Canyon sheeted zone  
539 define three distinct populations that match those seen in the three main units of  
540 the TIC (KC, HD, CP). They concluded that mechanical erosion, mixing of crystals,  
541 and magmatic redeposition played a dominant role in schlieren formation.

542

543 We suggest that these structures have several implications: (1) The reintrusion of  
544 magmatic structures by the surrounding magmas and overprinting of the structures  
545 by magmatic fabrics support the hypothesis that melt was present in the structures  
546 and the surrounding plutonic material when the structures formed; (2) magmatic  
547 structures preserve evidence for crystal sorting during local movement of magmas  
548 and thus that at least local non-static magma chambers existed; (3) the sharp  
549 truncations of compositionally-defined layers and subparallel mineral fabrics argue  
550 for erosion of crystal mushes and removal from the exposed plane of the eroded  
551 material. We find it very unlikely that strictly chemical processes formed the  
552 unusual model mineral proportions, the magmatic fabrics, and the sharp  
553 truncations; (4) the truncations, reintrusion and disruption of structures show that  
554 at the meter scale some materials were recycled into the surrounding magma  
555 mushes; and (5) the composition of the structures is best explained by crystal  
556 sorting of pre-mixed magmas and/or during erosion/recycling events.

557

558 **Mineral-scale examples of erosion/recycling**



559 The following evidence for mixing and recycling in the TIC occurs at the mineral  
560 scale. First, as noted above, a close inspection of single zircon ages indicates that the  
561 number of antecrystic zircons statistically increases from the older marginal units to  
562 the younger interior units (Memeti et al., 2014), and that the ages of the antecrystic  
563 zircons in the interior units always match the ages of the older, outer units of the  
564 TIC (e.g., Fig. 2). Rare xenocrystic zircons occur, but these are statistically minor and  
565 occur in samples from both outer and inner units. A very likely scenario to explain  
566 this zircon pattern is that as inner magma batches arrive in or ascend through older  
567 magma mush units, they incorporate zircons from these units.

568

569 A second observation is that some minerals that likely formed in older units are  
570 found in younger units and thus are antecrystic or cognate minerals (Fig. 13). For  
571 example we find 1-3 cm, euhedral hornblendes in the Cathedral Peak unit (Fig. 13a),  
572 which typically lacks or is poor in hornblende. Memeti et al. (2014) determined that  
573 these hornblendes are surrounded by a Cathedral Peak phase characterized by  
574 biotite and, even though they maintain their hornblende shape, are largely replaced  
575 by biotite. We thus interpret these to be hornblendes that formed in the Half Dome  
576 granodiorite and were recycled into Cathedral Peak magma, where they were  
577 unstable and pseudomorphed by biotite.

578

579 A potentially similar example is the presence of K-feldspar megacrysts in the late  
580 leucogranites, such as in the Johnson porphyry granite (Fig. 10). Megacrysts are not  
581 usually found in these leucogranites and the presence of resorbed and rounded

582 medium grained, biotite-bearing granodiorite around some megacrysts indicates  
583 that the megacrysts grew in Cathedral Peak magma before being recycled into the  
584 fine grained, biotite-poor leucogranites.

585

586 We have also suggested that some of the particularly large K-feldspar megacrysts in  
587 the outer parts of the Cathedral Peak (e.g., Memeti and Paterson, 2008) initially  
588 crystallized in the porphyritic Half Dome granodiorite and have continued their  
589 growth after being mixed into the Cathedral Peak magmas (Fig. 13c, d). This  
590 suggestion has yet to be fully tested.

591

592 Krause et al. (2009, 2010), Memeti et al. (2009, 2013, 2014), and Barnes et al.  
593 (2016) recently focused on the geochemistry of individual crystals, especially the  
594 geochemical zoning patterns of K-feldspars, but also plagioclase, hornblende, biotite,  
595 and titanite. The main results derived from electron microprobe x-ray element  
596 intensity mapping, and core-to-rim transects of electron microprobe spot and laser  
597 ablation-ICP-MS analyses are the following: (1) multiple populations with distinct  
598 crystal sizes and morphologies exist for some minerals (e.g., Solgadi and Sawyer,  
599 2008; Barnes et al., 2016); (2) all minerals preserve zones if slow diffusing elements  
600 are examined, and the number and character of growth zones differ both in different  
601 mineral populations and spatially throughout the TIC; (3) growth zones in some  
602 minerals such as K-feldspar preserve many repeated compositional patterns  
603 suggesting that either multiple magma batches were added to the magma chamber,  
604 or that crystals were repeatedly moved into different parts of the magma chamber

605 during growth (Memeti et al., 2014); (4) that multiple populations of each crystal,  
606 each with different trace element zoning patterns, are now mixed together at hand  
607 sample scale (Barnes et al., 2016), and (5) that simpler zoning and less  
608 heterogeneity (e.g., fewer different crystal populations) is preserved in crystals from  
609 the simpler and shorter duration lobes compared to rocks in the main TIC (Krause  
610 et al., 2009; Memeti et al., 2009, 2014). These authors proposed a model of crystals  
611 initially forming in different melt compositions and/or PT environments and then  
612 being mixed together into a new hybrid magma composition. Continued growth of  
613 minerals in the hybrid magma resulted in the similar REE patterns in rims of  
614 crystals that have different morphologies and mineral core chemistries.

615

## 616 **Discussion**

617 *Summary erosion/recycling:* We have summarized 7 datasets, listed below, all of  
618 which support the truncation and erosion of older magma mushes accompanied by  
619 recycling of some of the eroded materials into younger magma batches: (1) map  
620 patterns and characteristics of internal contacts that show local hybrid units,  
621 truncations, and evidence of removal of older units by younger; (2) widespread  
622 xenoliths and cognate inclusions, including “composite” examples; (3) widespread  
623 magmatic enclaves, including composite examples, plus local enclave swarms that  
624 also include xenoliths and cognate inclusions; (4) widespread schlieren-bounded  
625 magmatic structures showing evidence of truncations and erosion; (5) antecrystic  
626 zircons and other antecrystic minerals from older units now present in younger  
627 units; (6) whole rock compositions including elemental, REE, and isotopic data all

628 supportive of extensive mixing; and (7) mineral petrographic and geochemical  
629 studies indicating mixing of distinct populations based on crystal morphology,  
630 elemental chemical mapping, and REE core-to-rim transects. Even if interpretations  
631 for one or two of these examples might be questioned, the combination of all seven  
632 provides compelling evidence that the erosion of older magmatic units and recycling  
633 of eroded materials were widespread in the TIC.

634

635 This erosion/recycling occurred during repeated events over a range of spatial  
636 scales. For example, (1) a comparison of the Fletcher Peak and Kuna lobe maps  
637 shows that Kuna Crest units are truncated by a younger Kuna Crest unit, which in  
638 turn is truncated by a complex sheeted unit in the Fletcher Peak map, which in turn  
639 is truncated by a unit consisting of Half Dome granodiorite. These map patterns  
640 require at least 5 erosion/recycling events at the kilometer scale; (2) “composite”  
641 cognate inclusions require at least two erosion/recycling events; (3) repeated  
642 truncations of schlieren and subparallel magmatic fabrics in troughs support  
643 repeated erosion/recycling events at the 10 meter scale; (4) gradual increase in  
644 antecrystic zircons in younger units are most easily explained if repeated  
645 erosion/recycling events occurred since it is unlikely that all units were present and  
646 in a magmatic state at the same time.

647

648 *Spatial and temporal scales of these processes:* When only a few representative  
649 examples are presented, it is difficult to assess the total number and spatial  
650 distribution of different features in a pluton and thus determine the magnitude of

651 the inferred processes. We attempt to address this by estimating the approximate  
652 number, size and spatial distribution of the compositional and structural examples  
653 discussed above by extrapolating local examples to a pluton wide scale. Present  
654 topography allows us to examine vertical thicknesses of a few hundred to 3000  
655 meters. Since true vertical thicknesses are uncertain, volumes are difficult to  
656 determine: we therefore use the total number of objects, surface areas and lengths  
657 of internal contacts in the largely 2D exposure of the TIC as “reference frames” in  
658 this discussion. Our goal is a first order estimate of the numbers and spatial scales of  
659 the various examples of erosion and recycling discussed above.

660

661 The TIC is ~60-70 kilometers long and anywhere from 10 to 35 kilometers wide  
662 with a total surface area ~1,100 km<sup>2</sup>. Preserved surface areas of TIC units indicate  
663 that the Kuna Crest makes up 10%, the Half Dome 27%, the Cathedral Peak 58% and  
664 all leucogranites combined about 4% of the total area. If our interpretation that  
665 inner parts of the Kuna Crest and Half Dome units have been partially removed is  
666 correct, it is interesting to estimate the potential size of removed material. We have  
667 done so by using present exposures, evidence of truncated margins, location of  
668 cognate inclusions, zircon age distributions and guesses of the likely minimum and  
669 maximum extents of these units prior to intrusion of subsequent units (Fig. 14). We  
670 assume that the external margin of the Cathedral Peak and late leucogranites have  
671 not been changed because large, younger magma batches are not present.  
672 Throughout the entire growth history of the TIC, the minimum estimate of total  
673 removed area is ~595 km<sup>2</sup>, which is about 35% of the likely minimum original size

674 of the TIC. The maximum estimate is  $\sim 1295 \text{ km}^2$ , which is about 54% of original  
675 material removed from the TIC. If we assume a minimum 5 kilometer thickness over  
676 which removal of plutonic material occurred, then a minimum of  $2955 \text{ km}^3$  and  
677 maximum of  $11,975 \text{ km}^3$  of material was moved out of this 5 km section of the crust  
678 and/or recycled into younger units during the 10 m.y. lifespan of TIC. Internal (i.e.,  
679 within one magma unit), repeated erosion/recycling events might increase these  
680 numbers or simply reflect local recycling. The above estimates can be evaluated if  
681 we imagine that over 10 m.y. magmatic material was either removed by one or more  
682 volcanic eruptions, recycled into younger batches or by downward movement to  
683 deeper crustal levels in the magmatic system as younger batches ascended (Fig. 16).  
684 Volumes of volcanic eruptions in continental arcs range from  $0.1 \text{ km}^3$  to more than  
685  $1000 \text{ km}^3$  over average durations of  $\sim 50$  days (e.g. Simkin and Siebert, 1994). Thus  
686 three to 10 large eruptions, or a greater number of smaller volume eruptions could  
687 accommodate all of the removed materials. Total eruptive volumes in volcanic fields  
688 of similar dimensions and durations to the TIC range from 100s to 1000s of  $\text{km}^3$  of  
689 volcanic materials (Lipman 2008, Grunder et al., 2008). If some eroded material was  
690 recycled into younger magma batches, this would reduce the amounts of “removed”  
691 magma or plutonic material: below we estimate that potential magnitudes of  
692 recycled materials may range up to 25%. The magnitude of downward movement of  
693 magmatic/plutonic material is the least constrained.

694

695 Figure 1 displays the length of the main contacts in the TIC that are sharp at the  
696 meter scale, gradational over 10-100 meter scales, or are associated with hybrid

697 zones. The contact between Half Dome and Kuna Crest units is ~95 kilometers of  
698 which ~17% is sharp, 58% is gradational, and ~24% is associated with mappable  
699 hybrid units. The Cathedral Peak contact against older units is ~115 kilometers  
700 long, 50 kilometers of which forms discordant contacts with metamorphic host  
701 rocks. Of the remaining 65 kilometers (mostly against Half Dome units) 58% is  
702 sharp, 30% gradational and 12% is associated with hybrid units. The late  
703 leucogranites, although volumetrically small, have >>100 kilometers of contacts  
704 because of their thin elongate shapes. Greater than 70% of these contacts are sharp  
705 and the remaining are gradational. Clearly the Cathedral Peak contact is typically  
706 much more discordant than the Kuna Crest-Half Dome contacts. Thus field  
707 observations and geochronology indicate that the Cathedral Peak contact is typically  
708 an erosional contact with an age gap. The Kuna Crest-Half Dome contact, although  
709 mostly gradational or associated with hybrid zones, still preserves good evidence  
710 for truncation and erosion. But presumably the eroding magma batches and crystal  
711 mushes being eroded had enough melt to continue to interact both physically and  
712 chemically. Bergantz et al. (2015) recently modeled such behavior showing that  
713 crystal-rich systems can simultaneously behave as a "soft" viscoplastic material  
714 while failing in a Mohr-Coulomb fashion, thus forming linear (sharp) and diffusive  
715 (gradational) contacts during the same intrusive event.

716

717 Schlieren-bound troughs provide one example of local internal contacts associated  
718 with erosion in the TIC. We have measured >1000 troughs in local domains where  
719 detailed mapping was completed. If a conservative estimate of the spatial

720 distribution of troughs (number/km<sup>2</sup>) is extrapolated to entire units, we estimate a  
721 minimum number of >9000 troughs for the entire TIC. Contacts in these troughs  
722 range from 10s of centimeters to 100s meters in length: if we use a conservative  
723 average of 5 meter length/trough, then there is a minimum of 45 kilometers of  
724 internal trough contacts. Troughs tend to cluster (Memeti et al., 2014; Stanback et al.,  
725 2016). If we assume that one “event” causes 9 clustered troughs, then we need a  
726 minimum of 1000 “local events” to form the troughs in the TIC. We have also  
727 mapped 1-10 km-scale zones of fairly planar schlieren (Fig. 1) with local schlieren  
728 truncations that may be a form of broad trough or “magma mush avalanche”  
729 surfaces. Our estimates are that schlieren in these planar schlieren zones define  
730 around 17,000 kilometers of internal contacts and would require many 1000’s of  
731 events to form. In spite of these impressive lengths, if we assume that schlieren  
732 bands are around 5 centimeter thick on average, then all of the planar schlieren only  
733 make up about 0.85 km<sup>2</sup> in area or less than 1% of the total area of the TIC. Thus  
734 they represent a spectacular record of repeated erosion/recycling events in an  
735 active magma chamber but only have a minor effect on magma compositions.

736

737 It is equally intriguing to estimate the number of enclaves (Fig. 11), cognate  
738 inclusions (Fig. 7-11), and mixed minerals in the TIC and their scales of distribution.  
739 Using a conservative estimate established from field measurements of ~0.1  
740 enclave/m<sup>2</sup>, there are greater than 70 million exposed enclaves. Even if we  
741 drastically reduce this estimate, there are clearly millions of enclaves widely  
742 distributed throughout all three units. An estimate for the average area of a single



743 enclave is  $\sim 50 \text{ cm}^2$ . The calculated total area of enclaves for the exposed TIC is  
744 about  $0.0365 \text{ km}^2$  much less than 1% of the total area: thus the distribution of  
745 enclaves requires the formation and dispersal of a huge number of objects, although  
746 their total volume is small.

747

748 To date we have found evidence of mineral-scale mixing in almost every sample  
749 analyzed for ages or geochemistry. So far the only potential exceptions occur in the  
750 southern Half Dome lobe and in some late leucogranites. To exemplify the numbers  
751 of crystals involved we can make a preliminary estimate using zircons. We typically  
752 get  $>1000$  zircons in separates from  $\sim 1000 \text{ cm}^3$  samples. Assuming that  $\sim 10$  zircons  
753 occurred in any  $100 \text{ cm}^2$  surface cut in these samples, this number scaled to the  
754 entire TIC surface area, would imply around a trillion zircons. Memeti et al. (2014)  
755 noted that the number of antecrystic zircons increase in younger units and  
756 statistically make up around 25% of the total zircons in the inner Half Dome and  
757 Cathedral Peak units (Fig. 2a). This would imply that a minimum of 250 billion  
758 antecrystic zircons occur in the present surface exposure of the Half Dome and  
759 Cathedral Peak units. Even if this estimate is off by 2 orders of magnitude, there  
760 must be billions of antecrystic zircons mixed into the Half Dome and Cathedral Peak  
761 units.

762

763 All of the above measurements draw attention to the scale of the processes involved  
764 in erosion/recycling in the TIC. These processes likely involved erosion along 100s  
765 to 1000s of kilometers of contacts, during 1000s of “events” and involving 1000s of

766 cognate blocks, millions of enclaves and billions of antecrystic crystals, resulting in  
767 ~35-55% of material eroded from the present surface level, some (~25%? based on  
768 zircon estimates) recycled into younger batches and the majority displaced either  
769 up or down relative to the present surface.

770

771 *Location of erosion/recycling:* Where did this magmatic erosion and  
772 mixing/recycling occur? It is certainly possible that some occurred either at the site  
773 of magma generation in the lower crust/upper mantle or during magma ascent,  
774 although both of these would require that the source rocks and/or the units  
775 bordering the ascent path shared identical age and similar geochemical  
776 characteristics with the older TIC units exposed at the present crustal level. It is  
777 also possible that some recycling occurred at higher crustal levels and subsequently  
778 sank to the present levels. This would require a vertically connected magma  
779 plumbing system in a rheological state that would permit such sinking.

780

781 However, several observations suggest that a fair amount of erosion and recycling  
782 occurred at the presently exposed emplacement site. First, at the scale of 10s of  
783 kilometers, the presence of hybrid zones along the main internal contacts and  
784 truncations of units along these contacts seem to require, at least in part, in situ  
785 formation. The large scale, the consistent position between the two units with which  
786 the hybrid unit shares characteristics, and gradational contacts with these units  
787 would make it remarkably fortuitous if separate batches of magma were  
788 sequentially emplaced in the correct spatial order, or if the hybrid units formed

789 elsewhere and were transported to their present location as a package. We think it  
790 is more likely that the hybrid units represent in situ mixing between the adjacent  
791 units.

792

793 Second, Memeti et al. (2010) pointed out that the older, more isotopically primitive,  
794 shorter-lived southern lobes typically show significantly less evidence for mixing  
795 than similar units in the main plutonic body. If all recycling/mixing occurred during  
796 magma generation and ascent, then there is no reason that mixing should not be  
797 equally prevalent in these lobes.

798

799 Another intriguing, although less conclusive observation, concerns the composition  
800 of rocks making up local sheeted zones. For example, in both the Fletcher Peak (Fig.  
801 5) and Sawmill Canyon areas (Fig. 6), the zones of sheeting and mingling were partly  
802 formed from porphyritic Half Dome magmas, which is what would normally be the  
803 next innermost unit. But in both cases the porphyritic Half Dome (Fletcher Peak) or  
804 entire Half Dome (Sawmill Canyon) is entirely missing and instead younger units  
805 are now present. Thus one likely implication is that when these sheeted zones were  
806 forming, Half Dome magmas were present along the interior edges of these zones  
807 and were removed during intrusion of younger magma. The presence of Half Dome  
808 blocks and Half Dome aged zircons in these younger magmas supports this  
809 interpretation and, if correct, the implication that large volumes of plutonic material  
810 were eroded and removed.

811

812 At the meter to 10 meter scale, the preservation of numerous schlieren-bound  
813 magmatic structures, often with similar structural patterns (e.g., orientations,  
814 younging directions, migration directions) in the same spatial domains, also argue  
815 for in situ formation.

816

817 It is less certain where the dispersal of enclaves, xenoliths and cognate inclusions  
818 occurred, although the concentrations of these objects into “enclave swarms” likely  
819 occurred in situ. Many enclave swarms are one-half to a few meters wide and 10s of  
820 meters long, and like the magmatic structures, it seems highly unlikely that they  
821 moved any significant distance without being disrupted. We suspect that a great  
822 percentage of the millions of enclaves were formed and dispersed at significantly  
823 deeper crustal levels where conditions more favorable for widespread dispersal of  
824 mafic magmas exist, Preservation of disrupted and mingled mafic dikes occur in the  
825 TIC (Memeti and Paterson, 2007), but examples are widely distributed at the  
826 emplacement site (Fig. 11). Arguments about the origins of the cognate inclusions  
827 are the same as presented below for zircons in that it is uncertain where they  
828 formed but they either formed near the present emplacement level or their  
829 presence has implications for the types of materials being recycled from other  
830 locations. Finally, it is intriguing that the densities of many of these xenoliths and  
831 cognate inclusions are greater than the densities of the surrounding plutonic rocks,  
832 which were even lower densities when magma, implying that enclaves, most  
833 cognate inclusions, and mafic structures had negative buoyancies. This implies that

834 the combination of host magma viscosities and ascent rates must have been  
835 sufficient to bring the enclaves and xenoliths to their present sites and trap them.

836

837 The presence of antecrystic zircons in inner units implies either (1) zircons with  
838 identical ages occur in the magma source region, (2) zircons with identical ages  
839 occur in units making up the “host rock walls” that the magma ascended through, or  
840 (3) zircon was recycled at the emplacement site. The latter implies that more than  
841 one recycling event is needed to transport Kuna Crest zircons into the central parts  
842 of the Cathedral Peak. In spite of extensive TIMS and LA-ICP-MS dating of zircon  
843 cores and rims, statistically older zircon core ages have not been found (Memeti et  
844 al., 2010). Zircon saturation temperatures range from ~780 to ~710 °C (e.g., Miller  
845 et al., 2007), and these temperatures plus preserved antecrystic zircons suggest that  
846 zircon growth did not start early in the magma history. The present vertical  
847 thickness of the TIC is unknown: but the above observations suggest to us that most  
848 zircon mixing did not begin until magma ascent in the middle crust and during  
849 upper crustal emplacement.

850

851 Finally, although much more extensive single mineral geochemistry is needed, the  
852 presence of antecrystic zircons and preliminary observations show direct evidence  
853 that mixing of crystal populations is widespread (Krause et al., 2010; Memeti et al.,  
854 2014; Barnes et al., 2016). However where this mixing occurred is uncertain. The  
855 convergence of REE values in the rims of K-feldspar crystals suggests that at least  
856 the final mixing of these crystal populations occurred in hybrid melts that may be

857 preserved in the plutonic material at the present emplacement site. However, this  
858 hypothesis needs further testing (e.g., Barnes et al., 2016).

859

860 The above discussion suggests to us that some mixing of enclaves and crystals  
861 probably occurred by erosion/recycling/mixing during ascent but that a significant  
862 amount occurred at the present emplacement site. The preserved truncations,  
863 hybrid zones, local magmatic structures, cognate blocks, enclave and crystal mixing,  
864 and local enclave swarms and schlieren layers at the emplacement site indicates  
865 that these erosion and recycling/mixing processes occurred over an impressive  
866 range of scales during pluton growth. The likely result was removal of at least 35%  
867 of previous plutonic material from the present level of exposure and recycling of at  
868 least a component of this removed material into younger magmas.

869

870 *Size and number of TIC magma chambers:* Given the well established 10 m.y. growth  
871 history of the TIC, its irregular shape, and clear evidence of incremental growth, it is  
872 expected that at least several, and potentially many, ephemeral magma chambers  
873 existed (Fig. 14). All researchers would likely agree that individual batches formed  
874 at least short-lived magma chambers upon arrival. But there remains a great deal of  
875 debate about whether larger and longer lived magma chambers formed either  
876 because arriving batches were larger or that the rate of arrival of smaller batches  
877 was fast enough to allow coalescence into larger magma chambers (e.g., Michaut and  
878 Jaupart, 2006; Paterson et al., 2011). Our conclusion about the extent of

879 erosion/recycling supports the presence of large and active magma chambers and  
880 here we explore evidence for the number and size of potential magma chambers.  
881  
882 Memeti et al. (2010) used a combination of map patterns, TIMS U/Pb zircon ages,  
883 thermal modeling, magmatic fabric patterns, and bulk-rock compositional data to  
884 argue that each of the four TIC lobes at one time consisted of magma chambers  
885 roughly the size of the inner portions of the lobes (Fig. 14) and with hypersolidus  
886 durations of ~0.4 to 2.3 m.y. By comparing locations of steep gradients in a  
887 histogram plot of all TIMS single zircon ages from the TIC to the size of map regions  
888 with similar zircon ages, Memeti et al. (2014) also argued that large magma  
889 chambers grew in the main plutonic body at ~94 Ma (Kuna Crest magmas), 90.5 Ma  
890 (Half Dome magmas), and 88.5 Ma (Cathedral Peak magmas). If we link map  
891 patterns, contoured age distributions (e.g. Fig 1, 2 and Memeti et al., 2014), and the  
892 age spread of autocrystic zircons in dated samples, these data suggest that these  
893 latter magma chambers at one point were at least 100s km<sup>2</sup> in size with local  
894 hypersolidus durations of ½ to 1.5 m.y. and total hypersolidus histories of 1.5 to 2.5  
895 m.y (Fig. 14). The Kuna Crest and Half Dome magma chambers would have been  
896 centered in the SW to S part of the TIC (Fig. 14) whereas the Cathedral Peak magma  
897 chamber initially formed in the southern center of the TIC and then migrated  
898 northwards over several million years. Paterson et al. (2011) presented thermal  
899 models of the incremental growth of the TIC, which suggested that new batches  
900 arrived (assuming zircon crystallization ages give an approximate proxy for relative  
901 magma batch arrival times) in the locations where temperatures remained the

902 highest and presumably where the final crystallization of the previous magma  
903 chambers occurred. Both the zircon age patterns and the broad areas of similar  
904 biotite cooling ages of 91-90 Ma in the southern TIC and 88-86 Ma everywhere  
905 around the CP support this hypothesis (Fig. 1, 2).

906

907 Memeti et al. (2014) noted that in their zircon age cumulative probability curve, the  
908 distinct peaks at older ages (90 and 91 Ma) are due to the occurrence of antecrysts  
909 in younger units (particularly the Cathedral Peak), which is consistent with former  
910 larger magma batches of these ages being partially assimilated into the Cathedral  
911 Peak since these peaks “represent an overrepresentation of crystals of this age  
912 compared to the relatively small observable magma volume of the equigranular Half  
913 Dome granodiorite unit.” The evidence for erosion/recycling presented in this paper  
914 (e.g., cognate inclusions, “inner” magmatic material in sheeted zones, antecrystic  
915 zircons) supports this idea that the size of the original Kuna Crest and Half Dome  
916 magma chambers were significantly bigger than their present map patterns since  
917 their inner, crystal-poor parts are now partially removed or recycled (Fig. 14). This  
918 would not be the case for the Cathedral Peak and late leucogranites. Our estimates  
919 indicates that these magma chambers at one time reached areas > 500 km<sup>2</sup>.

920

921 The estimates of removed/recycled materials in the TIC have implications for  
922 calculating pluton-scale “tempos” of magmatism. Paterson et al. (2011) and Memeti  
923 et al. (2014, Figure 4-4) estimated volume addition rates during the 10 m.y. growth  
924 of the TIC. We have revised these suggested temporal histories to include the



925 minimum estimate of removed materials for older plutonic units (Fig. 14, 15). Our  
926 new estimate of the growth of the TIC (Fig. 15) suggests that the original volumes of  
927 the earlier Kuna Crest and Half Dome magma bodies were as large or larger than the  
928 Cathedral Peak body. Greater volume input of magma occurred every 3-4 m.y. If we  
929 assume (based on the antecrystic to autocrystic zircon ratio in younger units), that  
930 ~25% of the removed material is recycled into younger units, this would reduce the  
931 estimated additions for the Half Dome and Cathedral Peak magmas by around 5%  
932 on Figure 15.

933

934 A couple of issues remain unclear. Above we conclude that small magma chambers  
935 formed in the lobes and larger magma chambers formed in the main body of the TIC.  
936 It is not clear if the two magma chambers in the southern lobes were ever connected  
937 to those of similar age in the main body long enough to chemically and physically  
938 interact. Memeti et al. (2010) argue that the two northern lobes formed from  
939 magmas derived from one of the main magma chambers and the gradual northward  
940 younging age pattern supports this. Thus our working hypothesis is that there were  
941 two fairly disconnected magma chambers in southern lobes, at least three larger  
942 magma chambers in the main body that, before removal of their inner parts, reached  
943 sizes of  $>500 \text{ km}^2$  and that the locus of newly arriving magmas and/or of the  
944 remaining magma chambers migrated northward. The final large magma chamber  
945 occurred in the Cathedral Peak unit in the northeast corner of the TIC based on the  
946 young zircon and biotite ages and fairly evolved compositions in this region.

947

948 It is also unclear to what degree the large magma chambers in the main body grew  
949 from rapidly arriving smaller batches with very similar compositions, or from large  
950 batches (that may or may not have formed from amalgamation of smaller batches at  
951 depth). Contacts between potential batches that make up these former large magma  
952 chambers are not preserved. Detailed mapping and studies of single mineral  
953 compositional and zoning histories will be needed to fully evaluate this issue.

954

955 *Processes driving erosion/recycling:* If the above conclusions are correct, then a large  
956 amount of magmatic erosion and remixing occurred at upper-crustal depths during  
957 growth and final hypersolidus evolution of the TIC. Although Glazner (2014) argued  
958 that such magmatic erosion and mixing should rarely occur since erosion requires  
959 turbulent flows with high Reynolds numbers (Re), there are abundant examples  
960 both in nature and in elegant models of such erosion and remixing in magmatic  
961 systems (Ruprecht et al., 2008; Burgisser and Bergantz, 2011; Barboni and Schoene,  
962 2014; Bergantz et al., 2015). Three scenarios are worth mentioning: (1) In rare  
963 cases processes such as volatile increase may raise Re numbers to moderate values;  
964 (2) even at low Reynolds numbers there are processes that still operate to aid  
965 erosion and movement of materials; and (3) there are processes that can lead to  
966 erosion and mixing that do not rely on surface tractions or turbulent flow. Studies  
967 by Bachmann and Bergantz (2006), Michaut and Jaupart (2006), Ruprecht et al.  
968 (2008), Burgisser et al. (2011), Klemetti and Clynne (2014) and Cooper and Kent  
969 (2014) among others provide examples of processes driving the remobilization of  
970 magmas. Where gas bubbles provide the driving force, Re numbers can increase to

971 about ~100-400. However, even in models of magmatic systems with low to  
972 moderate Re numbers (e.g., 1-10), nonlinear terms remain important (Burgisser et  
973 al., 2005; Del Gaudio and Ventura, 2008; Burgisser and Bergantz, 2011; Dufek, pers.  
974 comm., 2014). Plus the increasing melt viscosities and low Stokes number of crystals  
975 in magmas with low Re numbers imply that the particles will follow any fluid  
976 motion fairly closely as drag coefficients go up (Burgisser et al., 2005; Burgisser and  
977 Bergantz, 2011; Dufek, person comm., 2014).

978

979 Equally important are processes in magmatic systems that can trigger erosion and  
980 remixing without the requirement of being driven by turbulent flows. For example,  
981 Bergantz et. al. (2015) and Schleicher et al. (2016) showed models of one magma  
982 batch intruding another during the temporal evolution of magma chambers that  
983 result in extensive visco-plastic collapse of older materials and mixing into younger  
984 batches. Such a process can drive convection (Martin et al., 1987) and downward  
985 flow of the older magma in part to make space for the newly arriving magma (Fig.  
986 16). Marsh (1996, 2006, 2013, 2015) has published a series of papers that explore  
987 the growth of solidification fronts in cooling magma chambers. If cooling is faster at  
988 the roof or upper levels of magma chambers, then these solidification fronts will  
989 form over-steepened and even overhanging zones of denser crystal mushes (Fig. 16)  
990 that are unstable and prone to collapse and avalanching into the hotter centers or  
991 onto rheological boundaries or floors of magma chambers (Žák and Paterson, 2010).  
992 Removal of magma and remixing may also occur during volcanic eruptions (Bacon  
993 and Lowenstern, 2005; Barboni and Schoene, 2014) or collapse of unstable steep

994 margins between magma batches (Bergantz, 2000). Furthermore, the negative  $\Delta V$   
995 during cooling of these crystal mush zones results in contraction and tearing, which  
996 can lead to erosion and movement along magmatic faults (Paterson, 2009;  
997 Humphreys and Holness, 2010). Synmagmatic tectonic straining of magma  
998 chambers may trigger faulting, erosion, and collapse of materials. Finally, the  
999 complex thermal and strain gradients within intrusive complexes can locally drive  
1000 stoping and erosion that may remove and recycle older material into younger  
1001 batches (e.g., Del Gaudio and Ventura, 2008; Paterson et al., 2011) and may cause  
1002 movement of local magma batches resulting in a wide variety of small-scale  
1003 magmatic structures (Paterson, 2009).

1004

1005 Figure 16 displays a cartoon of an idealized magma chamber with (1) growing  
1006 solidification fronts that are locally collapsing and in turn driving additional  
1007 magmatic erosion, mixing and redeposition, (2) arriving magma batches driving  
1008 convective stirring, return flow and mixing, and (3) a variety of resulting truncation  
1009 surfaces, displacement of crystal mushes, remixing, and the formation of local  
1010 magmatic structures. Observations presented above suggest that in the TIC 1000s  
1011 of such events, or a smaller number of large events resulting in 100s of subsidiary  
1012 localized events, occurred in a number of active magma chambers that rapidly  
1013 evolved in space and time during the growth of this batholith (Fig. 14, 15, 16).

1014

1015 **Processes during growth of the TIC**

1016 The upper-crustal Tuolumne Intrusive Complex grew incrementally over 10 m.y. by  
1017 a complex set of processes operating over a range of temporal and spatial scales.  
1018 Growth began with the emplacement of numerous, but volumetrically small magma  
1019 batches forming sheets of Kuna Crest magmas (Hardee, 1982; Memeti et al. 2010,  
1020 2014) followed by three periods of much larger magma additions, or pluton-scale  
1021 flare-ups, at approximately 94-93, 91-90 and 88-87 Ma either by numerous  
1022 chemically similar small batches or fewer but larger batches. During these flare-ups,  
1023 smaller magma chambers (up to 40 km<sup>2</sup>) formed in the lobes and larger magma  
1024 chambers (up to >500 km<sup>2</sup>) formed in the main part of the intrusive complex.  
1025 Irrespective of magma chamber size, repeated, multiscale, magmatic erosion events  
1026 of older intrusive units occurred in these magma chambers driven by a complex  
1027 interplay of buoyancy-driven intrusion of younger magma into older crystal mushes,  
1028 collapse and avalanching along growing solidification fronts, both broader and local  
1029 convection driven by internal thermal, compositional, and rheological gradients  
1030 (Martin et al., 1987) and by tectonic strains imposed on the magma chambers.  
1031 Certainly some of the implied erosion and mixing occurred at greater depths  
1032 resulting in the arriving magmas already being pre-mixed. The 1000s of “erosion  
1033 and recycling events” at the emplacement site resulted in removal of ~35-55% of  
1034 the original plutonic material in the presently exposed surface with a small portion  
1035 being recycled into younger magma batches.

1036

1037 *Implications:* The evidence that active magma chambers, some > 500 km<sup>2</sup>, can form  
1038 at upper crustal levels have a number of implications for generating the magma

1039 volumes and characteristics recorded by erupted volcanic materials (Bachmann et  
1040 al., 2005; Charlier et al., 2007; Barboni and Schoene, 2014). These observations  
1041 support models in which convection, mixing, and varied internal physical and  
1042 chemical gradients form significant compositional diversity at upper crustal levels.  
1043 The extensive mixing recorded in the TIC brings into question the interpretation of  
1044 whole rock elemental and isotopic data and certainly indicates that the  
1045 characteristics of parental magmas can be significantly modified at shallow crustal  
1046 levels. The extensive mixing and recycling present challenges for evaluating the  
1047 magnitude of fractionation and original melt compositions. Finally the suggested  
1048 removal of 35-55% of previous magmatic units in plutons will dramatically alter  
1049 volume estimates at arc scales of magma added to crustal columns and of the  
1050 volumes of magma migrating through individual magmatic systems. Both regional  
1051 and local estimates of magma additions will influence our understanding of the  
1052 thermal and geochemical evolution of the growth of plutons, whereas the former  
1053 may dramatically change estimates of magma additions during flare-ups and the  
1054 resulting crustal growth (e.g., Paterson and Ducea, 2015, Roberts et al., 2015).  
1055 Accurate estimates of magma addition rates are also necessary if accurate estimates  
1056 of crustal thickness, isostatic response, surface elevation and erosion rates of the arc  
1057 are to be determined (e.g., Lee et al., 2015).

1058

1059

1060

1061 **Acknowledgements**

1062 Paterson acknowledges support from NSF grants EAR-1019636, EAR-0537892 and  
1063 EAR-0073943 and USGS EDMAP grants G12AC20178 (supporting Wenrong Cao),  
1064 G13AC00120 (supporting Sean Hartman) and 03HQA0038 (supporting Vali Memeti)  
1065 for work in and around the TIC. Žák acknowledges support from the Czech Science  
1066 Foundation through Grant No. P210/12/1385 and support from Charles University  
1067 in Prague through project PRVOUK P44. We thank Mark Pecha, George Gehrels and  
1068 other scientists from Arizona LaserChron Center for help while using their  
1069 geochronology lab and Sean Hartman for help with drafting. We thank editor Cal  
1070 Barnes for extensive editorial suggestions and reviewers George Bergantz, and Eric  
1071 Klemetti for their very useful comments, all of which helped to improve the quality  
1072 of the manuscript.  
1073

1074 **References Cited:**

- 1075 Ardill, K.E., and Paterson, S.R., and Memeti, V. (2015) Schlieren-bound magmatic  
1076 structures formed by the unmixing of granitic magmas: a case study from  
1077 Pothole Dome, Sierra Nevada. EOS, American Geophysical Union, Fall Meeting  
1078 Supplement.
- 1079 Ague, J.J., and Brimhall, G.H. (1988) Regional variations in bulk chemistry,  
1080 mineralogy, and the compositions of mafic and accessory minerals in the  
1081 batholiths of California. Geological Society of America Bulletin, 100, 912–927.
- 1082 Bachmann, O., and Bergantz, G.W. (2004) On the Origin of Crystal-poor Rhyolites  
1083 Extracted from Batholithic Crystal Mushes. Journal of Petrology, 45, 8, 1565-  
1084 1582.
- 1085 Bachmann, O., Dungan, M.A. and Bussy, F. (2005) Insights into shallow magmatic  
1086 processes in large silicic magma bodies: the trace element record in the Fish  
1087 Canyon magma body, Colorado. Contributions to Mineralogy and Petrology 149,  
1088 338-349.
- 1089 Bachmann, O., and Bergantz, G.W. (2006) Gas percolation in upper-crustal silicic  
1090 crystal mushes as a mechanism for upward heat advection and rejuvenation of  
1091 near-solidus magma bodies. Journal of Volcanology and Geothermal Research,  
1092 149, 85–102. doi:10.1016/j.jvolgeores.2005.06.002.
- 1093 Bachmann, O., Charlier, B.L.A., and Lowenstern, J.B. (2007) Zircon crystallization and  
1094 recycling in the magma chamber of the rhyolitic Kos Plateau Tuff (Aegean arc):  
1095 Geology, 35, 1, 73–76. doi: 10.1130/G23151A.1.



- 1096 Bacon, C. R., and Lowenstern, J.B. (2005) Late Pleistocene granodiorite source for  
1097 recycled zircon and phenocrysts in rhyodacite lava at Crater Lake, Oregon.  
1098 Earth and Planetary Science Letters, 233, 3-4, 277-293.
- 1099 Barbarin, B. (1990) Plagioclase xenocrysts and mafic magmatic enclaves in some  
1100 granitoids of the Sierra Nevada Batholith, California. Journal of Geophysical  
1101 Research 95, 17747– 17756.
- 1102 Barbarin, B. (2005) Mafic magmatic enclaves and mafic rocks associated with some  
1103 granitoids of the central Sierra Nevada batholith, California: nature, origin, and  
1104 relations with the hosts. Lithos, 80, 155– 177.
- 1105 Barboni, M. & Schoene, B., 2014, Short eruption window revealed by absolute crystal  
1106 growth rates in a granitic magma. Nature Geosci. 7, 524\_528.
- 1107 Barnes, C.G., Memeti, V., and Coint, N. (2016) Deciphering magmatic processes in  
1108 calc-alkaline plutons using trace element zoning in hornblende. Special  
1109 collection: Perspectives on origins and evolution of crustal magmas. American  
1110 Mineralogist, 101, 328–342.
- 1111 Bartley, J.M., Coleman, D.S., Glazner, A.F. (2008) Incremental pluton emplacement by  
1112 magmatic crack-seal: Transactions of the Royal Society of Edinburgh, Earth  
1113 Sciences, 97, 383–396.
- 1114 Bateman, P. C. (1992) Plutonism in the central part of Sierra Nevada Batholith,  
1115 California, United States Geological Survey Professional Paper, 186 p.
- 1116 Bateman, P.C., and Chappell, B.W. (1979) Crystallization, fractionation, and  
1117 solidification of the Tuolumne Intrusive Series, Yosemite National Park,  
1118 California. Geological Society of America Bulletin, 90, 465-482.

- 1119 Bateman, P.C., Kistler, R.W., and D.L. Peck (1983) Geologic Map of the Tuolumne  
1120 Meadows Quadrangle, Yosemite National Park, California: U.S.G.S. Miscellaneous  
1121 Investigations Series, Map GQ-1570, scale 1:62,500, 1 sheet.
- 1122 Bergantz, G.W. (2000) On the dynamics of magma mixing by reintrusion:  
1123 implications for pluton assembly processes: *Journal of Structural Geology*, 22,  
1124 1297-1309.
- 1125 Bergantz G.W. and Breidenthal, R.E. (2001) Non-stationary entrainment and  
1126 tunneling eruptions: A dynamic template for eruption processes and magma  
1127 mixing *Geophysical Research Letters*, 28, 3075-3078.
- 1128 Bergantz, G.W., Schleicher, J.M. and Burgisser, A. (2015) Open-system dynamics  
1129 and mixing in magma mushes, *Nature Geosciences*, letters, DOI:  
1130 10.1038/NGEO2534.
- 1131 Burgisser, A. and Bergantz, G.W. (2011) A rapid mechanism to remobilize and  
1132 homogenize highly crystalline magma bodies. *Nature*, 471, 212-216.
- 1133 Burgisser, A., Bergantz, G.W. and Breidenthal, R.E. (2005) Addressing Complexity in  
1134 Laboratory Experiments: The Scaling of Dilute Multiphase Flows in Magmatic  
1135 Systems. *Journal of Volcanology and Geothermal Research*, Elsevier, 141, 3-4,  
1136 245-265.
- 1137 Bracciali, L., Paterson, S., Memeti, V., Rocchi, S., and Mundil, R. (2008) Filling the  
1138 magma chamber of the Tuolumne Batholith, Sierra Nevada, California: LASI III  
1139 conference: *Physical Geology of Subvolcanic Systems: Laccolith, Sills and Dykes*,  
1140 Elba Island.

- 1141 Burgess, S.D. (2006) Field, geochemical, and geochronologic study of the inner  
1142 Tuolumne Intrusive Series [Master of Science: San Jose State University, 155 p.
- 1143 Burgess, S.D., and Miller, J.S. (2008) Construction, solidification and internal  
1144 differentiation of a large felsic arc pluton: Cathedral Peak granodiorite, Sierra  
1145 Nevada Batholith, in Annen, C., and Zellmer, G.F., eds., Dynamics of crustal  
1146 magma transfer, storage and differentiation: Geological Society, London, Special  
1147 Publications, 304, 203–234.
- 1148 Charlier, B.L.A., Bachmann, O., Davidson, J.P., Dungan, M.A., & Morgan, D.J. (2007)  
1149 The upper crustal evolution of a large silicic magma body: Evidence from  
1150 crystal-scale Rb-Sr Isotopic heterogeneities in the Fish Canyon Magmatic  
1151 System, Colorado. *Journal. Petrology* 48, 1875-1894.
- 1152 Coleman, D.S. (2005) Field evidence for the assembly of the Half Dome Pluton by  
1153 amalgamation of small intrusions: Geological Society of America, Abstracts and  
1154 Programs, 37, 4.
- 1155 Coleman, D.S., and Glazner, A.F. (1997) The Sierra Crest Magmatic Event: Rapid  
1156 Formation of Juvenile Crust during the Late Cretaceous in California:  
1157 *International Geology Review*, 39, 9, 768 - 787.
- 1158 Coleman, D.S., Gracely, J.T., Gaschnig, R., Glazner, A.F., Bartley, J.M. (2008) Rethinking  
1159 how we map and date plutons: John Muir Intrusive Suite of the Sierra Nevada  
1160 Batholith: Geological Society of America, Abstracts with Programs, 40,1, 62.
- 1161 Coleman, D.S., Gray, W., and Glazner, A.F. (2004) Rethinking the emplacement and  
1162 evolution of zoned plutons; geochronologic evidence for incremental assembly  
1163 of the Tuolumne Intrusive Suite, California: *Geology*, 32, 5, 433-436.

- 1164 Cooper, K.M. and Kent, A.J.R. (2014) Rapid remobilization of magmatic crystals kept  
1165 in cold storage. *Nature* 506, 480-483.
- 1166 Crowley, J.L., Bowring, S.A., and Miller, R. (2006) Timescales of Magmatic Processes  
1167 in a 92 Ma Pluton Using High-Precision U-Pb ID-TIMS Zircon Geochronology: an  
1168 Example From the Half Dome Granodiorite, *Eos Trans. American Geophysical*  
1169 *Union, Fall Meeting Supplement* 87, 52, Abstract V54B-08.
- 1170 Crowley, J.L., and Bowring, S.A. (2007) Magma Chamber Dynamics From High-  
1171 Precision U- Pb Geochronology of Micro-Sampled Chemical Domains: *Eos Trans.*  
1172 *American Geophysical Union, Fall Meeting Supplement* 88, 52, Abstract V31G-  
1173 07.
- 1174 Del Gaudio, P., and Ventura, G. (2008) Mechanical erosion of xenoliths by magmatic  
1175 shear flow, *Geophysical Research Letters*, 35, *L09302*,  
1176 *doi:10.1029/2008GL033781*.
- 1177 Dufek, J., and Bergantz, G.W. (2007) Suspended load and bed-load transport of  
1178 particle-laden gravity currents: The role of particle–bed interaction: Theoretical  
1179 and Computational Fluid Dynamics, 21, 119–145, doi: 10.1007/s00162-007-  
1180 0041-6.
- 1181 Economos, R., Memeti, V., Paterson, S.R., Miller, J., Erdmann, S., Žák, J. (2009) Causes  
1182 of compositional diversity in a lobe of the Half Dome granodiorite, Tuolumne  
1183 batholith, Central Sierra Nevada, CA: *Earth and Environmental Science*  
1184 *Transactions of the Royal Society of Edinburgh*, 100, The Sixth Hutton  
1185 *Symposium on the Origin of Granites and Related Rocks*.

- 1186 Fernandez, A.N., and Gasquet, D.R. (1994) Relative rheological evolution of  
1187 chemically contrasted coeval magmas : example of the Tichka plutonic complex  
1188 (Morocco). *Contributions to Mineralogy and Petrology*, 116, 316-326.
- 1189 Fleck, R.J., and Kistler, R.W. (1994) Chronology of multiple intrusion in the  
1190 Tuolumne intrusive suite, Yosemite National Park, Sierra Nevada, California, in  
1191 Lanphere, M. A., Dalrymple, G. B., and Turrin, B. D., eds., U. S. Geological Survey  
1192 Circular, Report: C 1107: Reston, U. S. Geological Survey, 101 p.
- 1193 Fleck, R.J., Kistler, R.W., and Wooden, J.L. (1996) Geochronological complexities  
1194 related to multiple emplacement history of the Tuolumne intrusive suite,  
1195 Yosemite National Park, California, *Abstracts with Programs - Geological Society*  
1196 *of America*, Volume 28: Boulder, 65-66.
- 1197 Frost, T.P. and Mahood, G.A. (1987) Field, chemical, and physical constraints on  
1198 mafic-felsic magma interaction in the Lamarck granodiorite, Sierra Nevada,  
1199 California: *Geological Society of America Bulletin*, 99, 272-271.
- 1200 Glazner, A.F. (2014) Magmatic life at low Reynolds number. *Geology*,  
1201 doi:10.1130/G36078.1
- 1202 Glazner, A.F., Bartley, J.M., Coleman, D.S., Gray, W., and Taylor, R.Z. (2004) Are  
1203 plutons assembled over millions of years by amalgamation from small magma  
1204 chambers? *GSA Today*, 14, 4-5, 4-11.
- 1205 Glazner, A.F., Bartley, J.M., and Coleman, D.S. (2008) Magmatic crack-seal and why it  
1206 is difficult to recognize in plutons: LASI III Conference, Elba Island, *Abstracts*,  
1207 39-40.

- 1208 Gray, W., Glazner, A.F., Coleman, D., and Bartley, J. (2008) Long-term geochemical  
1209 variability of the Late Cretaceous Tuolumne Intrusive Suite, central Sierra  
1210 Nevada, California: Geological Society, London, Special Publications, 304, 183-  
1211 201, doi:10.1144/SP304.10.
- 1212 Grunder, A.L., Klemetti, E.W., Feeley, T.C., and McKee, C.M. (2008) Eleven million  
1213 years of arc volcanism at the Aucanquilcha Volcanic Cluster, northern Chilean  
1214 Andes: implications for the life span and emplacement of plutons: Transactions  
1215 of the Royal Society of Edinburgh: Earth Sciences, 97, 415–436.
- 1216 Hardee, H.C. (1982) Incipient magma chamber formation as a result of repetitive  
1217 intrusions: Bulletin of Volcanology, 45, 1, 41-49.
- 1218 Hildreth, W., 2004. Volcanological perspectives on Long Valley, Mammoth Mountain,  
1219 and Mono Craters: several contiguous but discrete systems. Journal of  
1220 Volcanology and Geothermal Research 136 (3–4), 169–198.
- 1221 Hodge, K.F., Carazzo, G., Montague, X., Jelinek, A.M. (2012) Magmatic structures in  
1222 the Tuolumne Intrusive Suite, California: a new mode for the formation and  
1223 deformation of ladder dikes: Contributions to Mineralogy and Petrology, DOI  
1224 10.1007/s00410-012-0760-6
- 1225 Huber, C., Bachmann, O. and Dufek, J. (2011) Thermo-mechanical reactivation of  
1226 locked crystal mushes: Melting-induced internal fracturing and assimilation  
1227 processes in magmas. Earth Planetary Science Letters, 304, 443-454.
- 1228 Huber, N.K., Bateman, P.C., and Wahrhaftig, C. (1989) Geologic Map of Yosemite  
1229 National Park and vicinity, California: U.S.G.S. Miscellaneous Investigations  
1230 Series Map I-1874, scale 1:125,000, 1 sheet.

- 1231 Humphreys, M.C.S. and Holness, M.B. (2010) Melt-rich segregations in the  
1232 Skaergaard Marginal Border Series: Tearing of a vertical silicate mush. *Lithos*  
1233 119, 181-192.
- 1234 Hutton, D.H.W. (1992) Granite sheeted complexes: evidence for the dyking ascent  
1235 mechanism: *Transactions Royal Society of Edinburgh Earth Sciences*, 83, 377-  
1236 382.
- 1237 Ickert, R.B., and Mundil, R. (2012), An objective method to determine the probability  
1238 distribution of the minimum apparent age of a sample of radio-isotopic dates:  
1239 American Geophysical Union Fall Meeting, abstract V23A-2796.
- 1240 Irmis, R.B., Mundil, R., Martz, J.W., and Parker, W.G. (2011) High-resolution U-Pb  
1241 ages from the Upper Triassic Chinle Formation (New Mexico, USA) support a  
1242 diachronous rise of dinosaurs: *Earth and Planetary Science Letters*, 309, 3-4,  
1243 258-267.
- 1244 Kistler, R.W. (1993) Mesozoic Intrabatholithic Faulting, Sierra Nevada, California: in  
1245 Mesozoic Paleogeography of the Western United States-II, Pacific Section SEPM,  
1246 Book 71, edited by Dunn, G., and McDougall, K., p. 247-262.
- 1247 Kistler, R.W. and Fleck, R.J. (1994) Field guide for a transect of the Central Sierra  
1248 Nevada, California: Geochronology and isotope geology: United States  
1249 Geological Survey Open File Report 94-267, 53 p.
- 1250 Kistler, R.W., Chappell, B.W., Peck, D.L., and Bateman, P.C. (1986) Isotopic variation  
1251 in the Tuolumne Intrusive Suite, central Sierra Nevada, California:  
1252 *Contributions to Mineralogy and Petrology*, 94, 204-220.
- 1253 Klemetti, E.W. and Clynne, M.A. (2014) Localized rejuvenation of a crystal mush

- 1254 recorded in zircon temporal and compositional variation at the Lassen volcanic  
1255 center, northern California. PLoS ONE 9, e113157.
- 1256 Krause, J., Memeti, V., Paterson, S.R. (2009) Examining the role of magma mixing  
1257 with major and minor element distribution patterns in rock-forming minerals  
1258 in the Tuolumne batholith, Sierra Nevada, CA: Eos Trans. American Geophysical  
1259 Union, Fall Meeting Supplement, 90 (52), Abstract # V42A-07.
- 1260 Krause, J., Memeti, V., and Paterson, S.R., (2010) Examining the role and relative  
1261 timing of magma mixing and fractionation in the formation of the Kuna Crest  
1262 lobe of the Tuolumne batholith, Sierra Nevada, USA: American Geophysical  
1263 Union Fall Meeting Supplement.
- 1264 Lee, C.-T.A., Turner, S., Paterson, S.R., Cao, W. (2015) The rise and fall of continental  
1265 arcs: interplays between magmatism, uplift, weathering, and climate. Earth and  
1266 Planetary Sciences Letters, 425, 105-119.
- 1267 Marsh, B.D. (1996) Solidification fronts and magmatic evolution. Mineralogical  
1268 Magazine, 60, 5-40.
- 1269 Marsh, B.D. (2006) Dynamics of Magma Chambers. Elements, 2, 287-292.
- 1270 Marsh, B.D. (2013) On some fundamentals of igneous petrology. Contributions to  
1271 Mineralogy and Petrology (2013) 166:665–690, DOI 10.1007/s00410-013-  
1272 0892-3.
- 1273 Marsh B.D (2015) Magmatism, Magma, and Magma Chambers. In: Gerald Schubert  
1274 (editor-in chief) Treatise on Geophysics, 2nd edition, Vol 6. Oxford: Elsevier;  
1275 2015. p. 273-323.



- 1276 Martin, D., Griffiths, R.W., and Campbell, I.H. (1987) Compositional and thermal  
1277 convection in magma chambers: Contributions to Mineralogy and Petrology, 96,  
1278 465–475, doi: 10.1007/BF01166691.
- 1279 Mattinson, J.M. (2001) Multi-Step High-Resolution Pb/U and Pb/Pb Zircon Age  
1280 Spectra: Combined Annealing, Partial Dissolution, and TIMS Analysis: American  
1281 Geophysical Union Fall Meeting Supplement 82, 47, abstract V22C-1056.
- 1282 Mattinson, J.M. (2003) CA (Chemical Abrasion) - TIMS: High-Resolution U-Pb Zircon  
1283 Geochronology Combining High-Temperature Annealing of Radiation Damage  
1284 and Multi-Step Partial Dissolution Analysis: American Geophysical Union Fall  
1285 Meeting Supplement 84, 46, abstract V22E-06.
- 1286 Mattinson, J.M. (2005) Zircon U–Pb chemical abrasion (“CA-TIMS”) method:  
1287 Combined annealing and multi-step partial dissolution analysis for improved  
1288 precision and accuracy of zircon ages: Chemical Geology, 220, 47-66.
- 1289 Matzel, J., Mundil, R., Paterson, S., Renne, P., and Nomade, S. (2005) Evaluating  
1290 pluton growth models using high resolution geochronology: Tuolumne  
1291 Intrusive Suite, Sierra Nevada, CA: Geological Society of America Abstracts with  
1292 Programs, 37, .7, 56-10.
- 1293 Matzel, J., Miller, J.S., Mundil, R., and Paterson, S.R. (2006a) Zircon saturation and the  
1294 growth of the Cathedral Peak pluton, CA: Geochimica Et Cosmochimica Acta, 70,  
1295 18, A403.
- 1296 Matzel, J., Mundil, R., Renne, P.R., Paterson, S.R. (2006b) Using  $^{40}\text{Ar}/^{39}\text{Ar}$   
1297 thermochronology to track the thermal evolution of the Tuolumne Batholith,

- 1298 Sierra Nevada, CA: Eos Trans. American Geophysical Union, Fall Meeting  
1299 Supplement 87, 52, Abstract V51E-1715.
- 1300 Matzel, J., Miller, J., Mundil, R., Wooden, J., Mazdab, F., Paterson, S.R., and Memeti, V.  
1301 (2007a). Zircon growth and recycling during the assembly of the Tuolumne  
1302 batholith, Sierra Nevada, CA. Geological Society of America: Abstracts with  
1303 Programs, 103<sup>rd</sup> Cord. Section meeting.
- 1304 Matzel, J., Mundil, R., Miller, J., Wooden, J., Mazdab, F., Paterson, S.R., and Memeti, V.  
1305 (2007b) Growth of the Tuolumne Batholith: Zircon Crystallization Temperature,  
1306 Age and Trace Element Data. EOS Trans. American Geophysical Union, 88 52,  
1307 Fall Meeting Supplement, Abstract V44C-08.
- 1308 Memeti, V. (2009) Growth of the Cretaceous Tuolumne batholith and synchronous  
1309 regional tectonics, Sierra Nevada, CA: A coupled system in a continental margin  
1310 arc setting: PhD Dissertation, University of Southern California, 300 pp.
- 1311 Memeti, V. and Paterson, S.R (2007) Enclave formation, dispersion and  
1312 accumulation in the Kuna Crest lobe of the Tuolumne Batholith, central Sierra  
1313 Nevada, California: Geological Society of America Abstracts with Programs, 39,  
1314 6, 224.
- 1315 Memeti, V., Paterson, S.R. (2008) Heterogeneous Kfs megacryst size and abundance  
1316 variation in the northern Cathedral Peak lobe, Tuolumne batholith: Cordilleran  
1317 Section meeting 2008, Las Vegas. Geological Society of America Abstracts with  
1318 Programs, 40, 1, 74.
- 1319 Memeti, V., Krause, J., and Paterson, S.R. (2009) Deciphering magma chamber  
1320 processes in the Tuolumne intrusion and its lobes using element distribution

- 1321 maps of single minerals: Geological Society of America Abstracts with Programs,  
1322 41, 7, 59.
- 1323 Memeti, V., Paterson, S., Matzel, J., Mundil, R., and Okaya, D. (2010) Magmatic lobes  
1324 as "snapshots" of magma chamber growth and evolution in large, composite  
1325 batholiths: An example from the Tuolumne intrusion, Sierra Nevada, California:  
1326 Geological Society of America Bulletin, 122, 1912–1931, doi:10.1130/B30004.1
- 1327 Memeti, V., Paterson, S.R., Krause, J., Mundil, R. (2011) Incremental growth of a large,  
1328 long lived magma chamber: Batholith to mineral scale evidence for mixing,  
1329 recycling and fractionation processes in the Tuolumne batholith, California,  
1330 USA: VII Hutton Symposium on Granites and Related Rocks, Avila, Spain, 4-9  
1331 July 2011, eds. J.F. Molina, J.H. Scarrow, F. Bea, and P. Montero, p. 98.
- 1332 Memeti, V., Barnes, C.G., Krause, J., and Paterson, S.R. (2013) Crystal Cocktails in the  
1333 Tuolomne Intrusive Complex. Geological Society of America: Abstracts with  
1334 Programs 45, 7, 230.
- 1335 Memeti, V., Paterson, S.R., Mundil, R. (2014) Day 4: Magmatic Evolution of the  
1336 Tuolumne Intrusive Complex, in Memeti, V., Paterson, S., and Putirka, K. (eds.),  
1337 Formation of the Sierra Nevada Batholith: Magmatic and Tectonic Processes  
1338 and Their Tempos: Geological Society of America Field Guide 34, 43–74,  
1339 doi:10.1130/2014.0034(04).
- 1340 Michaut, C. and Jaupart, C. (2006) Ultra-rapid formation of large volumes of evolved  
1341 magma. *Earth and Planetary Sciences Letters*, 250, 38-52.

- 1342 Miller, J.S., Matzel, J.E.P., Miller, C.F., Burgess, S.D., and Miller, R.B. (2007) Zircon  
1343 growth and recycling during the assembly of large, composite arc plutons:  
1344 Journal of Volcanology and Geothermal Research, 167, 1-4, 282-299.
- 1345 Miller, R.B., and Paterson, S.R. (2001) Construction of mid-crustal sheeted plutons:  
1346 Examples from the north Cascades, Washington: Geological Society of America  
1347 Bulletin, 113, 11, 1423-1442.
- 1348 Mundil, R., Brack, P., Meier, M., Rieber, H., and Oberli, F. (1996) High resolution U-Pb  
1349 dating of Middle Triassic volcanoclastics: Time-scale calibration and verification  
1350 of tuning parameters for carbonate sedimentation: Earth and Planetary Science  
1351 Letters, 141, 1-4, 137-151.
- 1352 Mundil, R., Metcalfe, I., Ludwig, K.R., Renne, P.R., Oberli, F., Nicoll, R.S. (2001) Timing  
1353 of the Permian–Triassic biotic crisis: implications from new zircon U/Pb age  
1354 data (and their limitations): Earth and Planetary Science Letters, 187, 131-145.
- 1355 Mundil, R., Ludwig, K.R., Metcalfe, I., and Renne, P.R. (2004a) Age and timing of the  
1356 Permian mass extinctions: U/Pb dating of closed-system zircons: Science, 305,  
1357 5691, 1760-1763.
- 1358 Mundil, R., Nomade, S., Paterson, S, and Renne, P.R. (2004b) Geochronological  
1359 constraints (  $^{40}\text{Ar}/^{39}\text{Ar}$  and U/ Pb) on the thermal history of the Tuolumne  
1360 Intrusive Suite (Sierra Nevada, California). EOS Trans. American Geophysical  
1361 Union, Fall Meeting Supplement, 85, 47.
- 1362 Pabst, A.(1928) Observations on inclusions in the granitic rocks of the Sierra Nevada.  
1363 University of California Publications, 17, 325– 386.
- 1364 Paterson, S.R. (2009) Magmatic tubes, troughs, pipes, and diapirs: Late-stage

- 1365 convective instabilities resulting in complex permeable networks in crystal-rich  
1366 magmas of the Tuolumne Batholith, Sierra Nevada, California: *Geosphere*, 5; 6;  
1367 496-527; DOI: 10.1130/GES00214.1.
- 1368 Paterson, S. R., and Vernon, R. H. (1995) Bursting the bubble of ballooning plutons: A  
1369 return to nested diapirs emplaced by multiple processes: *Geological Society of*  
1370 *America Bulletin*, 107, 11, 1356-1380.
- 1371 Paterson, S.R., and Ducea, M. (2015) Arc magmatic tempos: Gathering the evidence.  
1372 *Elements* 11, 91-98.
- 1373 Paterson, S.R., Fowler, T., Schmidt, K., Yoshinobu, A., and Yuan, S. (1998)  
1374 Interpreting Magmatic fabric patterns in plutons. *Lithos*, 44, 1-2, 53-82;  
1375 doi:10.1016/S0024-4937(98)00022-x.
- 1376 Paterson, S., Okaya, D., Matzel, J., Memeti, V., and Mundil, R. (2007) Size and  
1377 longevity of magma chambers in the Tuolumne batholith: A comparison of  
1378 thermal modeling and cooling thermochronology: *EOS Trans. American*  
1379 *Geophysical Union*, v. 88, n. 52, Fall Meeting Supplement , Abstract V44C-02.
- 1380 Paterson, S.R., Žák, J. and Janoušek, V. (2008) Growth of complex magmatic zones  
1381 during recycling of older magmatic phases: the Sawmill Canyon area in the  
1382 Tuolumne Batholith, Sierra Nevada, California. *Journal of Volcanology and*  
1383 *Geothermal Research*; doi: 10.1016/j.jvolgeores.2008.06.024.
- 1384 Paterson, S.R., Okaya, D.A., Memeti, V., Mundil, R., Lackey, J., Clemens-Knott, D.  
1385 (2009) Thermal models, stable isotopes and cooling ages from the  
1386 incrementally constructed Tuolumne batholith, Sierra Nevada: why large

- 1387 chambers did exist: Eos Trans, American Geophysical Union, Fall Meeting  
1388 Supplement 90 (52), Abstract # T24C-04.
- 1389 Paterson, S., Okaya, D., Memeti, V., Economos, R., Miller, R. (2011) Magma addition  
1390 and flux calculations of incrementally constructed magma chambers in  
1391 continental margin arcs: combined field, geochronologic, and thermal modeling  
1392 studies: Geosphere, 7, 1439-1468; doi:10.1130/GES00696.1
- 1393 Pitcher, W.S. and Berger, A.R. (1972) The Geology of Donegal: a Study of Granite  
1394 Emplacement and Unroofing, Wiley, New York, 435 p.
- 1395 Reid, J.B., Evans, O.C., Fates, D.G., 1983. Magma mixing in granitic rocks of the central  
1396 Sierra Nevada, California. Earth and Planetary Science Letters 66, 243–261.
- 1397 Reid, J.B., Murray, D.P., Hermes, O.D., and Steig, E.J. (1993) Fractional crystallization  
1398 in granites of the Sierra Nevada: How important is it? Geology, 21, 587-590.
- 1399 Roberts, N.M.W., Van Kranendonk, M., Parman, S., Shirey, S. and Clift, P.D. EDs (2015)  
1400 Continent Formation Through Time. Geological Society, London, Special  
1401 Publications, 389, 1–16. First published online November 13 2014,  
1402 <http://dx.doi.org/10.1144/SP389.13>
- 1403 Ruprecht, P., Bergantz, G.W., & Dufek, J. (2008) Modeling of gas-driven magmatic  
1404 overturn: Tracking of phenocryst dispersal and gathering during magma mixing.  
1405 Geochemistry, Geophysics, Geosystems, 9, Q07017, doi:10.1029/2008GC002022.
- 1406 Schleicher, J.M., Bergantz, G.W. Breidenthal, R.E. and Burgisser A. (2016) Time scales  
1407 of crystal mixing in magma mushes, Geophysical Research Letters 43,  
1408 doi:10.1002/2015GL067372.

- 1409 Schöpa, A. and Annen, C.J. (2013) The effects of magma flux variations on the  
1410 formation and lifetime of large silicic magma chambers. *Journal of Geophysical*  
1411 *Research - Solid Earth*, 118, 926-942.
- 1412 Simkin, T., and Siebert, L.(1994) *Volcanoes of the World*: Geoscience Press, Tucson,  
1413 Arizona, 349 p.
- 1414 Sisson, T.W. (2005) Solidification, zoning, and homogenization in Sierran plutons:  
1415 *Geological Society of America Abstracts with Programs*, 37, 4, 39.
- 1416 Solgadi, F., and Sawyer, E.W. (2008) Formation of igneous layering in granodiorite  
1417 by gravity flow: a field, microstructure and geochemical study of the Tuolumne  
1418 Intrusive Suite at Sawmill Canyon, California. *Journal of Petrology*, 49, 11, 2009-  
1419 2042, doi:10.1093/petrology/egn056.
- 1420 Stanback ,J.F., Ardill, K.E., Alisino, P.H. and Paterson, S.R. (2016) Crystal-mush flow  
1421 dynamics in migrating tubes in the Glen Aulin region of the Tuolumne Intrusive  
1422 Complex, *Geological Society of America Abstracts with Programs*. Vol. 48, No.  
1423 4 doi: 10.1130/abs/2016CD-274640
- 1424 Stern, T.W., Bateman, P.C., Morgan, B.A., Newell, M.F., and Peck, D.L. (1981) Isotopic  
1425 U-Pb ages of zircon from the granitoids of the central Sierra Nevada, California:  
1426 U. S. Geological Survey, Professional paper 1185.
- 1427 Titus, S.J., Clark, R., Tikoff, B. (2005) Geologic and geophysical investigation of two  
1428 fine-grained granites, Sierra Nevada Batholith, California: Evidence for  
1429 structural controls on emplacement and volcanism: *Geological Society of*  
1430 *America Bulletin* 117, 1256-1271.

- 1431 Tobisch, O.T., Fiske, R.S., Saleeby, J.B., Holt, E., and Sorenson, S.S. (2000) Steep tilting  
1432 of metavolcanic rocks by multiple mechanisms, central Sierra Nevada,  
1433 California: Geological Society of America Bulletin, 112, 7, 1043-1058.
- 1434 Tobisch, O.T., McNulty, B.A., and Vernon, R.H. (1997) Microgranitoid enclave swarms  
1435 in granitic plutons, central Sierra Nevada, California. Lithos, 40, 321-339.
- 1436 Vignerresse, J. L., and Bouchez, J. L. (1997) Successive granitic magma batches during  
1437 pluton emplacement: the case study of Cabeza de Araya, Spain: Journal of  
1438 Petrology, 38,12, 1767-1776.
- 1439 Walker, B.A. Jr., Miller, C.F., Claiborne, L., Wooden, J.L., Miller, J.S. (2007) Geology and  
1440 geochronology of the Spirit Mountain batholith, southern Nevada: Implications  
1441 for timescales and physical processes of batholith construction: Journal of  
1442 Volcanology and Geothermal Research 167, 239–262.
- 1443 Wallace, G.S. and Bergantz, G.W. (2002) Wavelet-based correlation (WBC) of zoned  
1444 crystal populations and magma mixing, Earth Plan. Sci. Letters, 202, 133-145.
- 1445 Wallace, G. S. and Bergantz, G.W. (2005) Reconciling heterogeneity in crystal zoning  
1446 data: An application of shared characteristic diagrams at Chaos Crags, Lassen  
1447 volcanic center, California. Contributions to Mineralogy and Petrology 149, 98,  
1448 112.
- 1449 Whittington, A.G., Hofmeister, A.M., and Nabelek, P.I. (2009) Temperature-dependent  
1450 thermal diffusivity of the Earth's crust and implications for magmatism: Nature,  
1451 458, doi:10.1038/nature07818.



- 1452 Wiebe, R.A. and Collins, W.J. (1998) Depositional features and stratigraphic sections  
1453 in granitic plutons: implications for the emplacement and crystallization of  
1454 granitic magma: *Journal of Structural Geology*, 20, 9/10, 1273-1289.
- 1455 Žák, J. and Paterson, S.R. (2005) Characteristics of internal contacts in the Tuolumne  
1456 Batholith, central Sierra Nevada, California (USA): Implications for episodic  
1457 emplacement and physical processes in a continental arc magma chamber:  
1458 *Geological Society of America Bulletin*, 117, 9/10, 1242-1255, doi:  
1459 10.1130/B25558.1.
- 1460 Žák, J. and Paterson, S.R. (2010) Magmatic erosion of the solidification front during  
1461 reintrusion: the eastern margin of the Tuolumne batholith, Sierra Nevada,  
1462 California: *International Journal of Earth Sciences*, 99, 801-812, DOI:  
1463 10.1007/s00531-009-0423-7.
- 1464 Žák, J., Paterson, S. R. and Memeti, V. (2007) Four magmatic fabrics in the Tuolumne  
1465 batholith, central Sierra Nevada, California (USA): Implications for interpreting  
1466 fabric patterns in plutons and evolution of magma chambers in the upper crust:  
1467 *Geological Society of America Bulletin* 119, 1/2, 184–201, doi: 10.1130/B25773.
- 1468 Žák, J., Paterson, S.R., Janoušek, V., Kabele, P. (2009) The Mammoth Peak Sheeted  
1469 complex, Tuolumne Batholith, Central Sierra Nevada, California: A Record of  
1470 Initial Growth or Late Thermal Contraction in a Magma Chamber?:  
1471 *Contributions to Mineralogy and Petrology*, 158, 447-470, doi 10.1007/s00410-  
1472 009-0391-8.
- 1473  
1474

1475

1476 Figure Captions

1477 Figure 1: Geologic map of the Tuolumne Intrusive Complex showing the main  
1478 compositional units and U/Pb zircon ages (after Memeti et al., 2010) and the  
1479 styles of the main internal contacts. Red line shows geochronologic transect  
1480 shown in Figure 2b. Boxes show locations of detailed maps in Figs 3-6.

1481

1482 Figure 2: (A) U/Pb CA-TIMS single zircon ages from sample KCL.536 (Kuna Crest  
1483 Lobe) representative of outer TIC units as well as the southern lobes and  
1484 sample CTP.11 (Cathedral Peak sample) representative of inner TIC units.  
1485 Outer units display uniform clusters of autocrystic zircons with rare  
1486 xenocrysts or antecrysts, whereas inner units contain zircons that are  
1487 significantly older than the predominant zircon population and have ages that  
1488 are similar to the ages of the older parts of the TIC (Memeti et al., 2010, 2014)  
1489 (B)  $^{40}\text{Ar}/^{39}\text{Ar}$  biotite ages from coarse and fine-grained biotites along a  
1490 southern transect (red line in Fig. 1) after Matzel et al. (2005). Note the step in  
1491 ages between two more gently dipping sections of the curve, the latter  
1492 indicating large regions of similar biotite cooling ages in the Half Dome  
1493 granodiorites. These cooling ages match the U/Pb zircon crystallization age of  
1494 the Half Dome and Cathedral Peak magmas, respectively.

1495

1496 Figure 3: Geologic map of the Glen Aulin area along the western edge of the TIC (Fig.  
1497 1). Mapping completed by Vali Memeti, Bob Miller, Scott Paterson and Jiří Žák.  
1498 Contact symbols same as in Fig. 1. Note the discontinuous hybrid zone between  
1499 the Glen Aulin tonalite (Kuna Crest) and equigranular Half Dome granodiorite  
1500 and truncations of older by younger magmatic units. Locally the Cathedral  
1501 Peak granite cuts across Half Dome units and directly intrudes the Glen Aulin  
1502 tonalite. PCT = Pacific Crest Trail. Mapping in Figures 3, 4, 5, 6 all completed at  
1503 1:10,000 to 1:5,000 scales.

1504

1505 Figure 4: Geologic map of the Kuna Crest lobe (Fig. 1) after Memeti et al. (2010).  
1506 Note truncation of compositionally defined zones KC-I and KC-II at the  
1507 northwest end of the lobe by east-west striking Kuna Crest units in the main  
1508 magma chamber. Also note the hybrid unit (tHD = Kuna Crest-Half Dome mix)  
1509 in the center of the lobe.

1510

1511 Figure 5: Geologic map of the Fletcher Peak area at the southern end of the TIC (Fig.  
1512 1) redrafted after Žák et al. (2005). Contact symbols same as in Fig. 1. The  
1513 east-west striking Kuna Crest unit is probably connected to the east-west  
1514 striking KK-III unit in Figure 4. In the Fletcher Peak area this unit is bordered  
1515 and locally truncated by a complex hybrid zone and in turn bordered by the  
1516 porphyritic Half Dome. Except locally within the hybrid zone, the equigranular  
1517 Half Dome unit is absent here.

1518

1519 Figure 6: (A) Geologic map of part of the eastern margin of the TIC west of  
1520 Saddlebag Lake (Fig. 1) and (B) the Sawmill Canyon area (mapped at 1:5,000  
1521 scale after Paterson et al., 2009). Mapping completed by Scott Paterson and Jiří  
1522 Žák. Contact symbols are the same as in Fig. 1. In (A) note that the Kuna Crest  
1523 unit does not extend north of the Sawmill Canyon area and only two pieces of  
1524 the Half Dome unit are found north of Sawmill Canyon. In (B) complex, sheeted,  
1525 east-west striking hybrids of porphyritic Half Dome and Cathedral Peak  
1526 magmas cut across and truncate north-south striking equigranular Half Dome  
1527 and Kuna Crest units. These hybrid units are truncated along their western  
1528 ends by a hybrid, locally hornblende-bearing Cathedral Peak unit.

1529

1530 Figure 7: Photos of recycled materials in the Kuna Crest units. Figure a, shows an  
1531 example of Paleozoic metasedimentary stoped blocks; Figure b shows older  
1532 plutonic, volcanic and mafic enclaves in a large mafic enclave now in a Kuna  
1533 Crest matrix; Figure c, d, and e show “composite” blocks of Jurassic volcanic  
1534 blocks (c, e) and calc-silicate metasediments (d), respectively surrounded by  
1535 mafic Kuna Crest tonalite in more felsic Kuna Crest granodiorite. Figure f  
1536 displays numerous cognate inclusions, mafic enclaves and rare xenoliths in a  
1537 hybrid Kuna Crest granodiorite.

1538

1539 Figure 8: Photos of recycled materials in Half Dome units. Figures a and b, show  
1540 examples of metavolcanic and metasedimentary xenoliths in Half Dome  
1541 granodiorite. Figures c and d show composite cognate inclusions where former  
1542 enclave swarms with local xenoliths are surrounded by a matrix of Kuna Crest  
1543 magmas and now reside in equigranular Half Dome granodiorite. Note the  
1544 sharp boundaries defining the rectangular shapes that cut and truncates  
1545 individual enclaves indicating that a former more elongate enclave swarm (e.g.,  
1546 Tobisch et al., 1997) was broken apart into rectangular pieces presumably  
1547 during movement of the Half Dome magma. Figure e displays a composite  
1548 block of volcanic rock locally attached to and intruded by Kuna Crest magma  
1549 now surrounded by a Half Dome matrix. Figure f shows a collection of  
1550 xenoliths, a large cognate inclusion of layered plutonic rock and enclaves near  
1551 the Kuna Crest – Half Dome contact.

1552

1553 Figure 9 shows examples of inclusions residing in the Cathedral Peak granodiorite.  
1554 Figure a shows a folded metavolcanic xenolith, Figure b a cognate inclusion of  
1555 Half Dome granodiorite, Figure c a layered cognate inclusion of porphyritic  
1556 Half Dome magma and Figure d a composite inclusion of layered plutonic rock  
1557 rimmed by Half Dome magma in the Cathedral Peak granodiorite. Figure e  
1558 shows a schlieren-bound tube sharply truncated by Cathedral Peak magma and  
1559 f shows an example of a composite inclusions with a small piece of layered

1560 plutonic rock in a matrix of layered Half Dome granodiorite (HD), now entirely  
1561 surrounded by Cathedral Peak granodiorite.

1562

1563 Figure 10 shows examples of various pieces of the Cathedral Peak granodiorite in  
1564 the Johnson granite. Figure a shows Cathedral Peak K-feldspar megacryst  
1565 antecrysts, Figure b an angular piece of Cathedral Peak granodiorite, and  
1566 Figures c and d rounded (partially melted?) pieces of Cathedral Peak  
1567 granodiorite, each with one large K-feldspar megacryst. Photos c and d taken  
1568 by Laura Bracciali (see also Bracciali et al., 2008).

1569

1570 Figure 11: Photos of enclaves and enclave swarms. Figure a is a mafic quartz diorite  
1571 dike intruding Kuna Crest granodiorite that is the same composition of many  
1572 enclaves in the Kuna Crest. Figure b a similar dike to Figure a, but now broken  
1573 apart and forming enclaves. Figure c depicts dispersed elliptical enclaves in the  
1574 Half Dome granodiorite. Figure d shows an enclave swarm with local cognate  
1575 inclusions and xenoliths. Figure e shows a composite enclave with a finer  
1576 grained mafic center, rimmed by a medium grained granodiorite, now residing  
1577 in Kuna Crest granodiorite. Figure f depicts a cognate block of a former enclave  
1578 swarm. Note sharp edge to the block that cuts across individual enclaves.

1579

1580 Figure 12: Photos of truncated and likely eroded/reintruded and partially recycled  
1581 magmatic structures. Figures a and b show repeated mafic schlieren defining  
1582 two sets of Cathedral Peak magmatic troughs with examples of sharp  
1583 truncations of older schlieren layers. These truncations are visible at the  
1584 centimeter scale and sharply cut across both mafic and felsic layers as well as  
1585 subparallel magmatic mineral foliations with no deflection of the older layers.  
1586 A new magmatic foliation is subparallel to the new, cross-cutting schlieren  
1587 layer. Figure c shows a package of mafic-felsic schlieren layers of Half Dome  
1588 granodiorite that show excellent grading of mafic minerals and are sharply  
1589 truncated by younger batches of magma. Figure d shows schlieren in  
1590 porphyritic Half Dome granodiorite sharply truncated by younger schlieren  
1591 layers. Figure e shows an example of a “bifurcated” schlieren-bound migrating  
1592 tube(s) that show repeated truncations of older tube margins by younger  
1593 margins and now surrounded by and locally reintruded by Cathedral Peak  
1594 granodiorite. Figure f displays an example in Cathedral Peak granodiorite of  
1595 planar schlieren and subparallel magmatic foliation truncated by, and  
1596 presumably removed during formation of a schlieren bound trough in which a  
1597 new schlieren parallel foliation is formed.

1598

1599 Figure 13: Photos of likely recycled antecrystic minerals. Figures a and b are former  
1600 large euhedral hornblendes, typical of the Half Dome units, now replaced by  
1601 biotite and surrounded by Cathedral Peak granodiorite, Figures c and d show

1602 large, zoned, isolated K-feldspar megacrysts, some of which have been  
1603 interpreted to form in porphyritic Half Dome magmas and are now recycled  
1604 into Cathedral Peak granodiorite.

1605

1606 Figure 14: Cartoon showing our interpretation of the former minimum (stippled)  
1607 and maximum (no pattern) extents (in yellow) of removed parts of the TIC for  
1608 Kuna Crest (A) and Half Dome (B) units resulting in the present configuration  
1609 (C). For each panel, black ellipses show estimated size, position and age of  
1610 inferred Kuna Crest (A), Half Dome (B) and Cathedral Peak (C) magma  
1611 chambers based on age distributions and the minimum extents of removed  
1612 materials. See text for discussion of evidence of these magma chambers.

1613

1614 Figure 15: A comparison of magma additions (in km<sup>2</sup>) versus age (95 – 85 Ma) in the  
1615 TIC based on the extent of present-day exposures and inferred former extents  
1616 of units prior to removal. If estimates of removed material are approximately  
1617 correct, then the areas or volumes of Kuna Crest and Half Dome magmas were  
1618 equal to or greater than the Cathedral Peak magmas. Either curve also implies  
1619 that the magma addition rates to the TIC were episodic and that three  
1620 prominent increases in magma additions occurred around 94-93 Ma, 91-90 Ma,  
1621 and 88-87 Ma.

1622



1623 Figure 16: Cartoon of an idealized magma chamber showing a number of potential  
1624 processes that would lead to erosion of older units, mixing of older and  
1625 younger crystal mushes, recycling of older materials into younger batches, and  
1626 formation of local magmatic structures. See text for discussion.



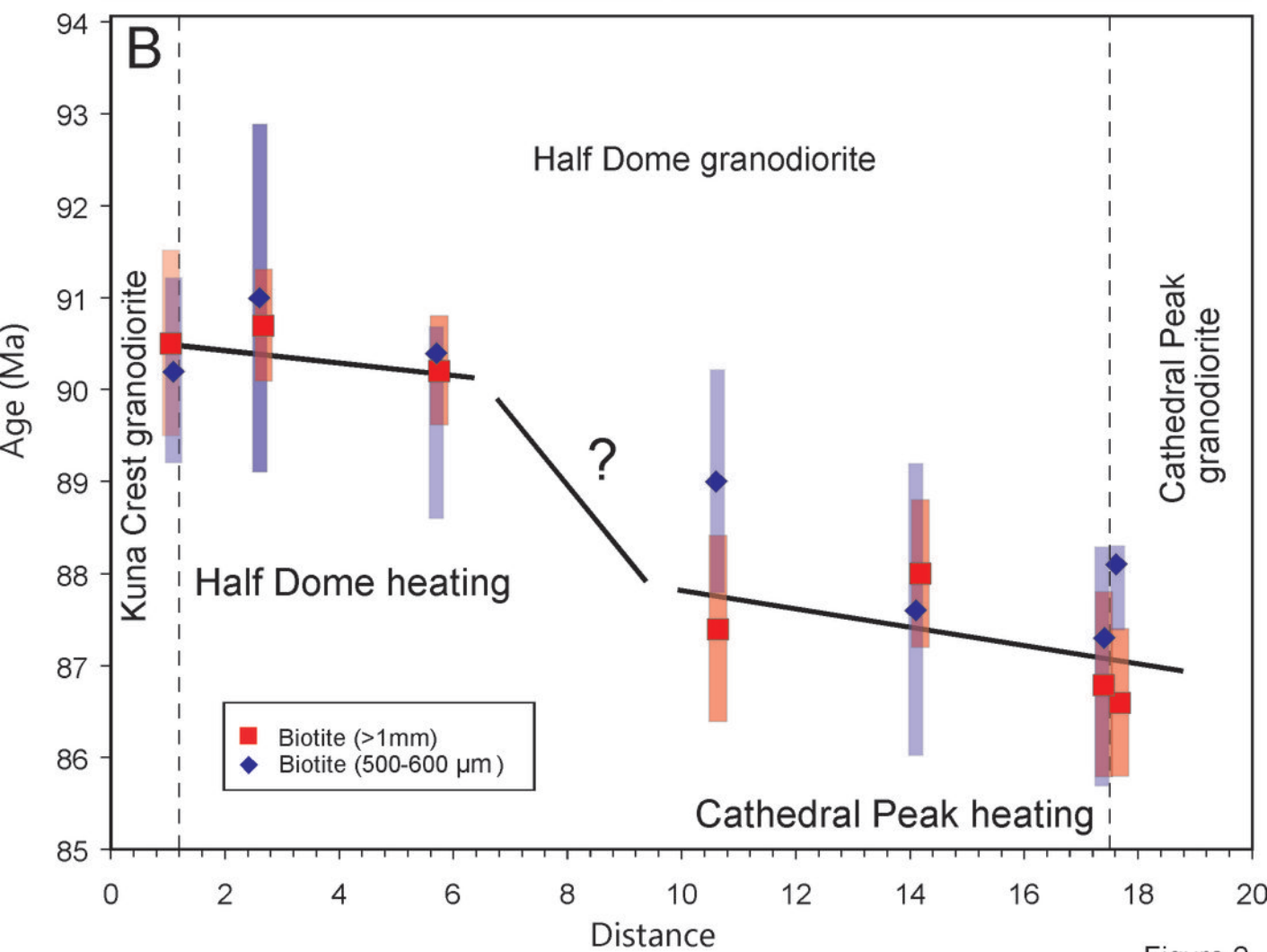
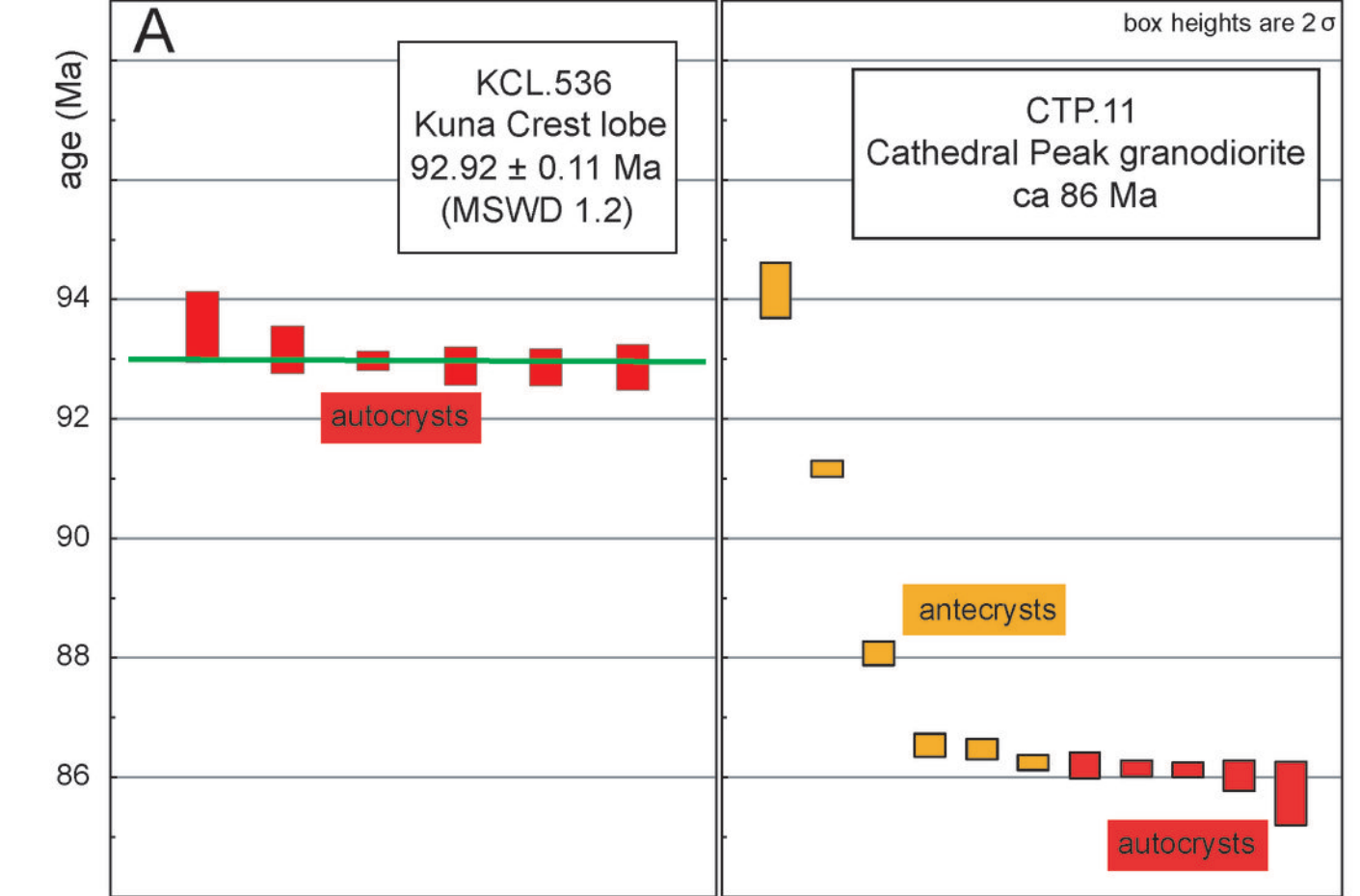
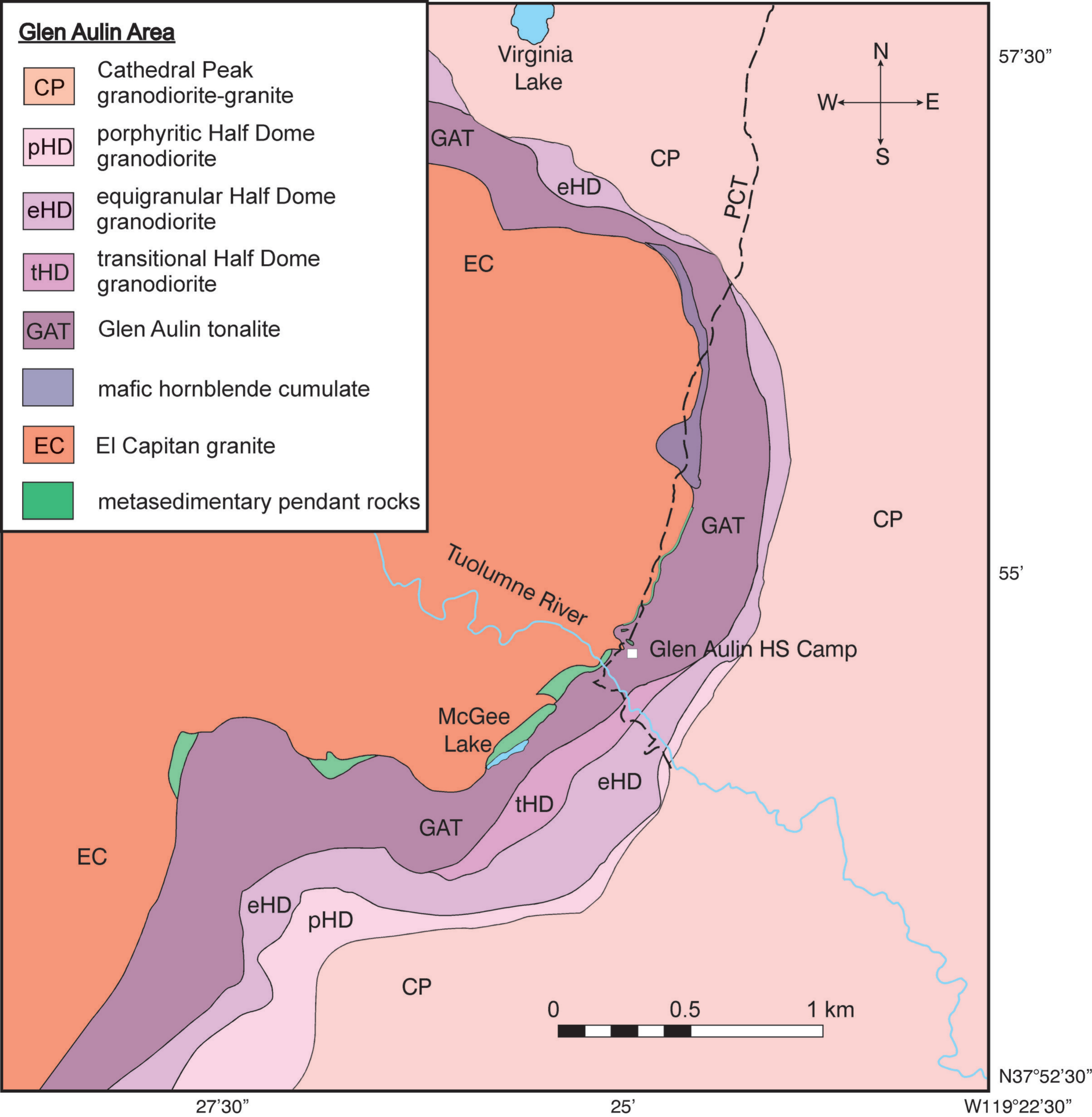


Figure 2

**Glen Aulin Area**

- CP Cathedral Peak granodiorite-granite
- pHD porphyritic Half Dome granodiorite
- eHD equigranular Half Dome granodiorite
- tHD transitional Half Dome granodiorite
- GAT Glen Aulin tonalite
- mafic hornblende cumulate
- EC El Capitan granite
- metasedimentary pendant rocks



**Figure 3**

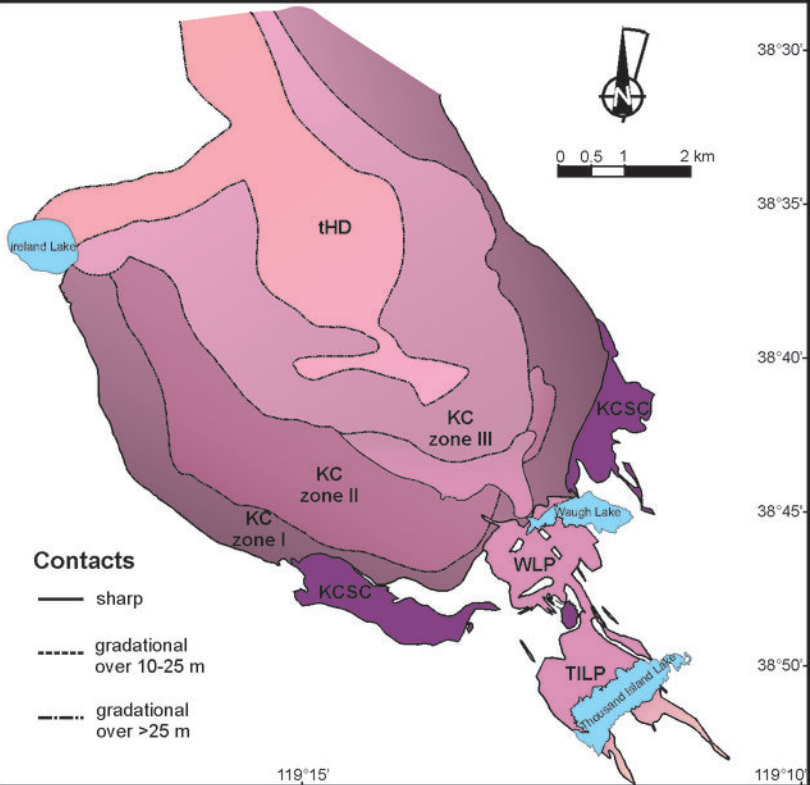


Figure 4

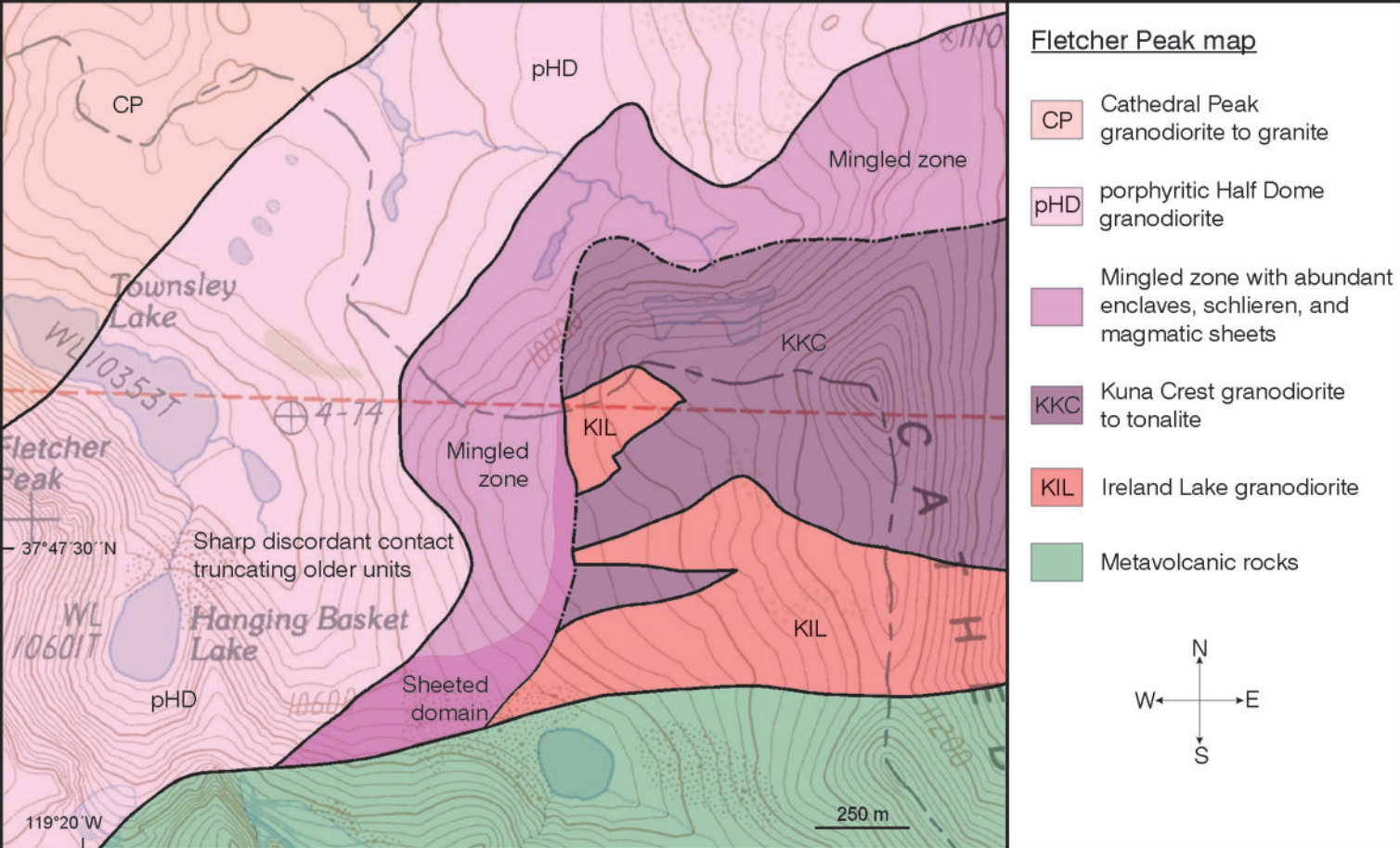


Figure 5

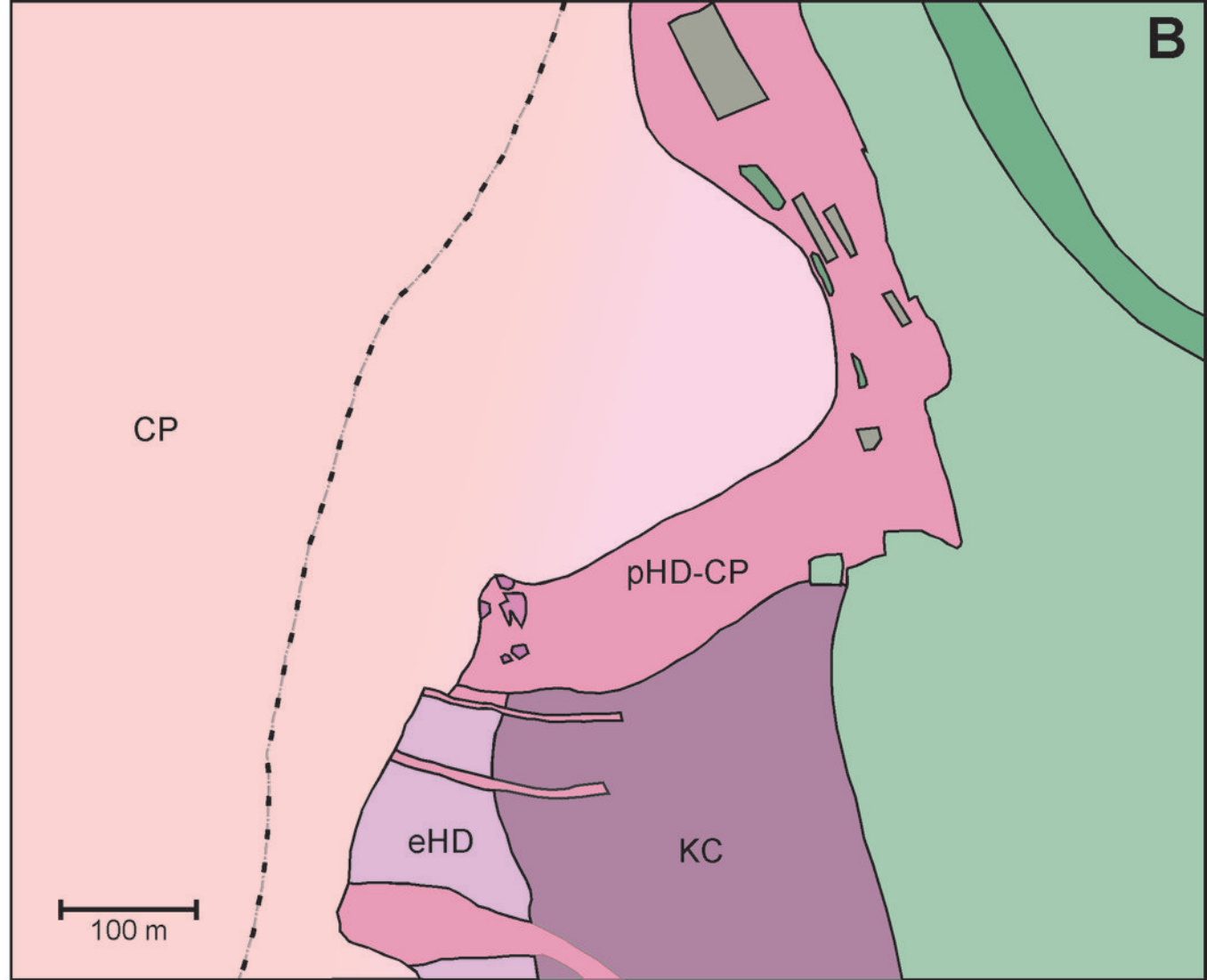
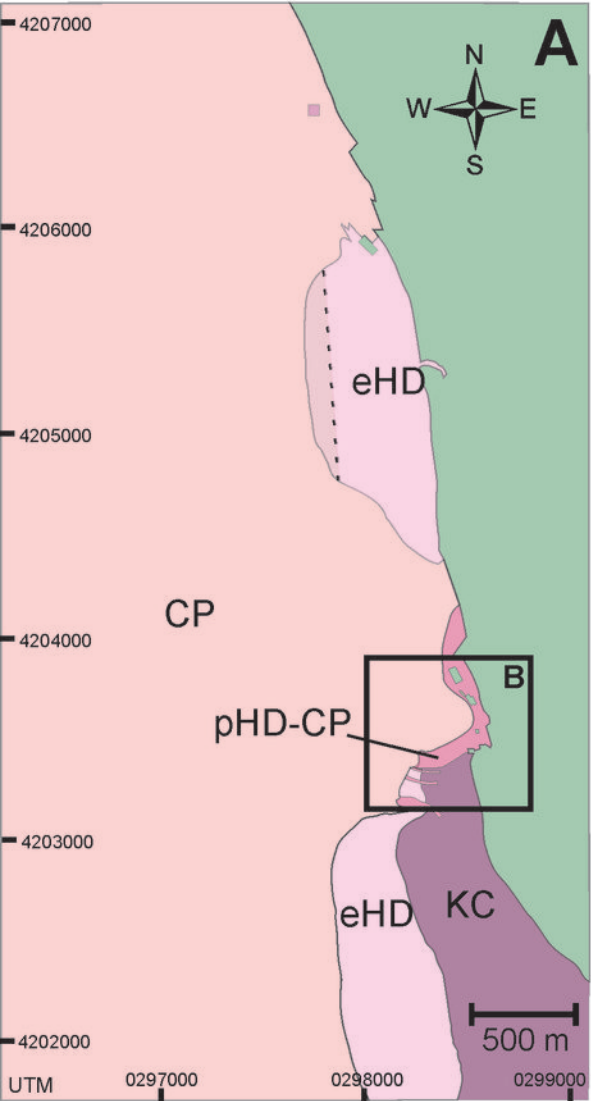


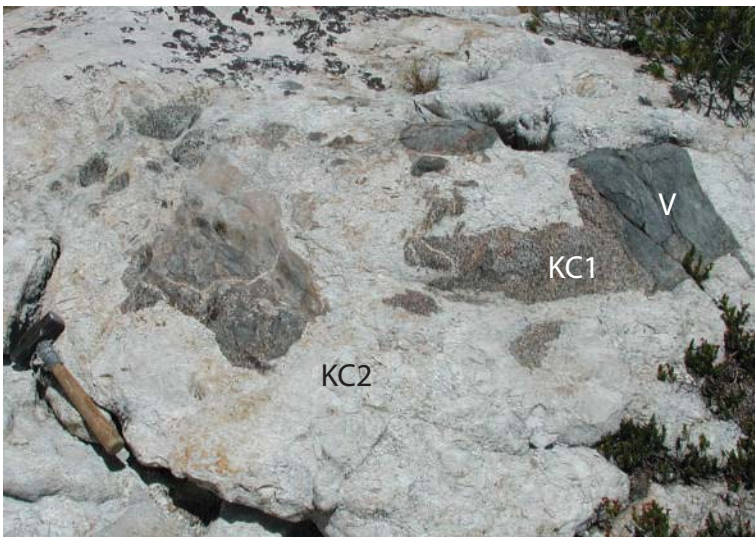
Figure 6



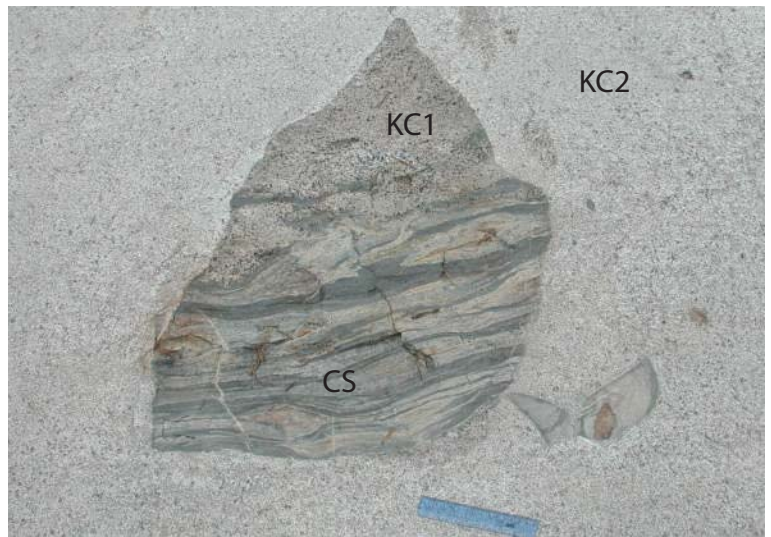
(a)



(b)



(c)



(d)



(e)



(f)

Figure 7





(a)



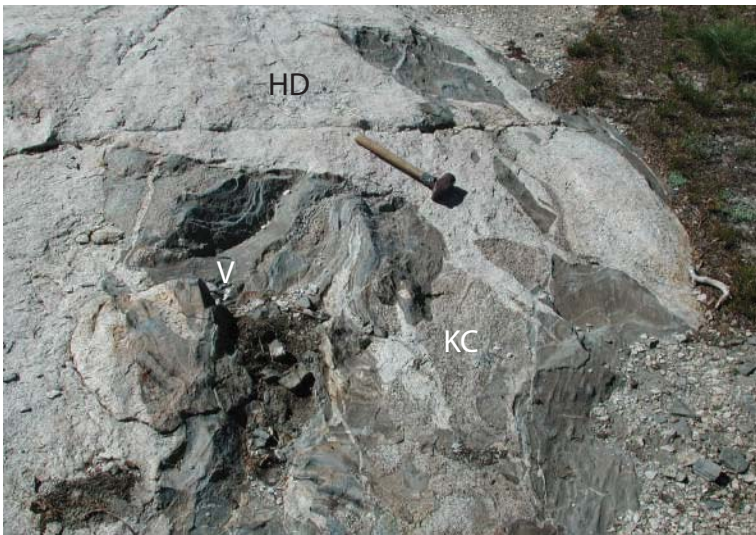
(b)



(c)



(d)



(e)



(f)

Figure 8



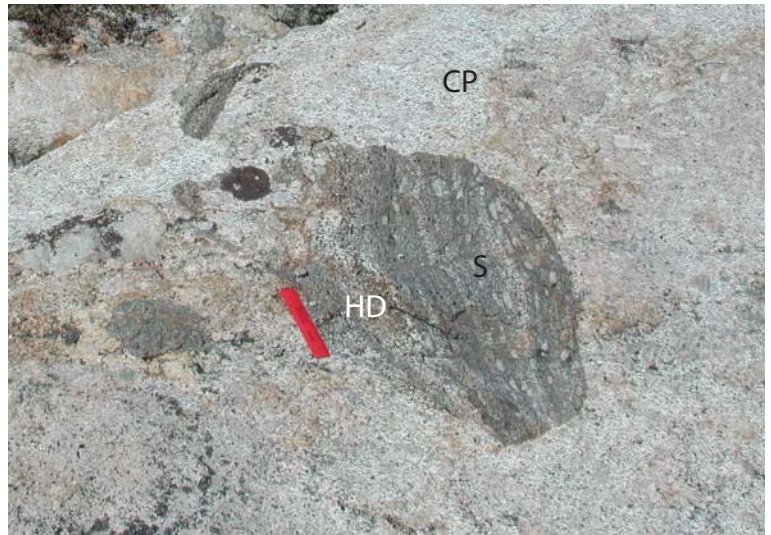
(a)



(b)



(c)



(d)

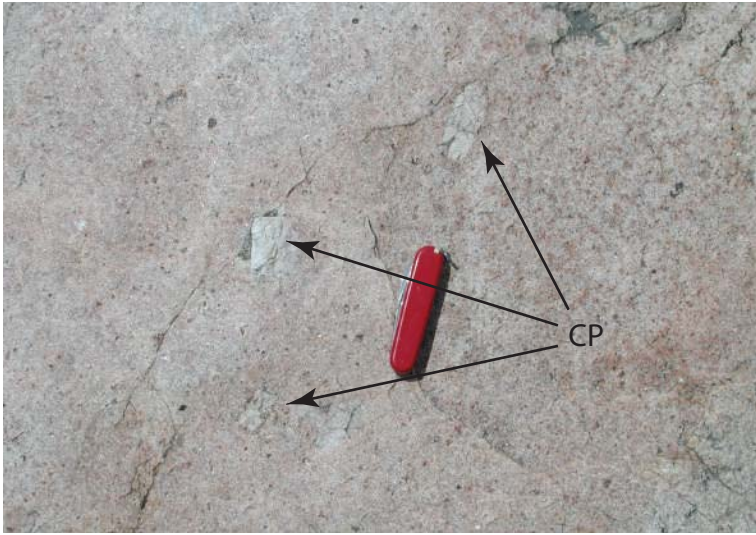


(e)



(f)

Figure 9



(a)



(b)



(c)



(d)



(a)



(b)



(c)



(d)



(e)



(f)

Figure 11



(a)



(b)



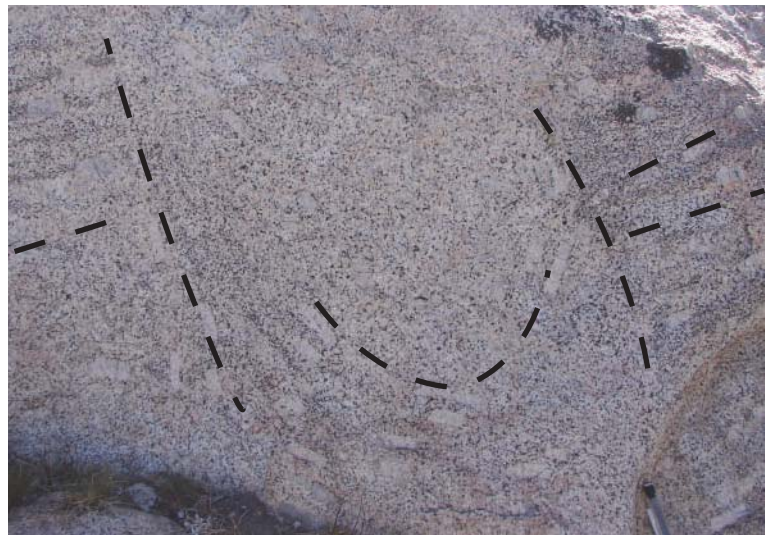
(c)



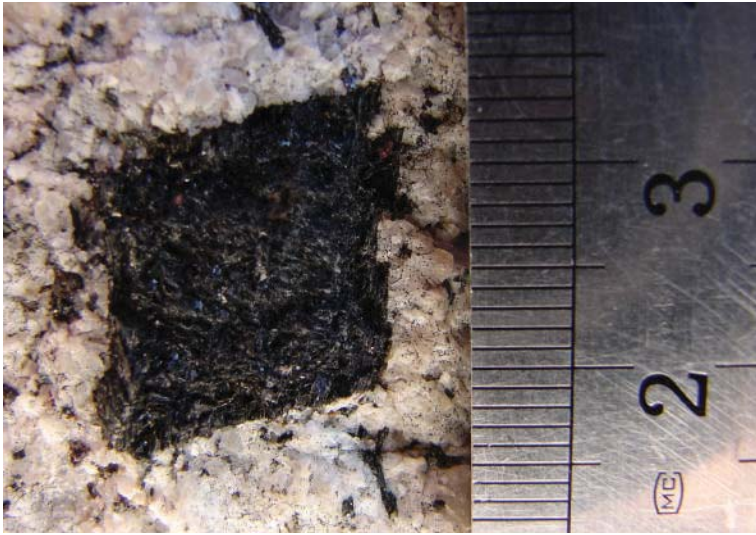
(d)



(e)



(f)



(a)



(b)



(c)



(d)

Figure 13

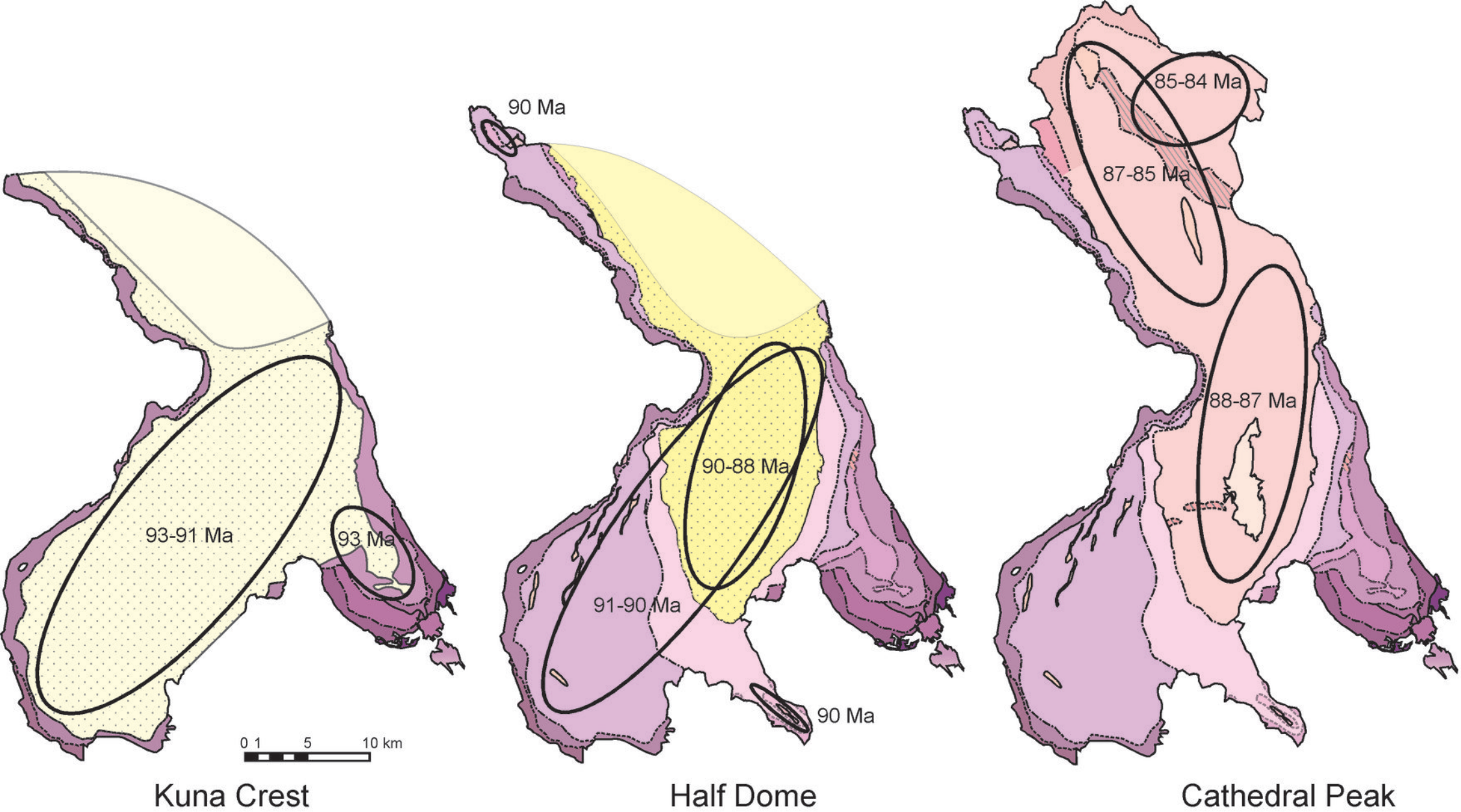


Figure 14

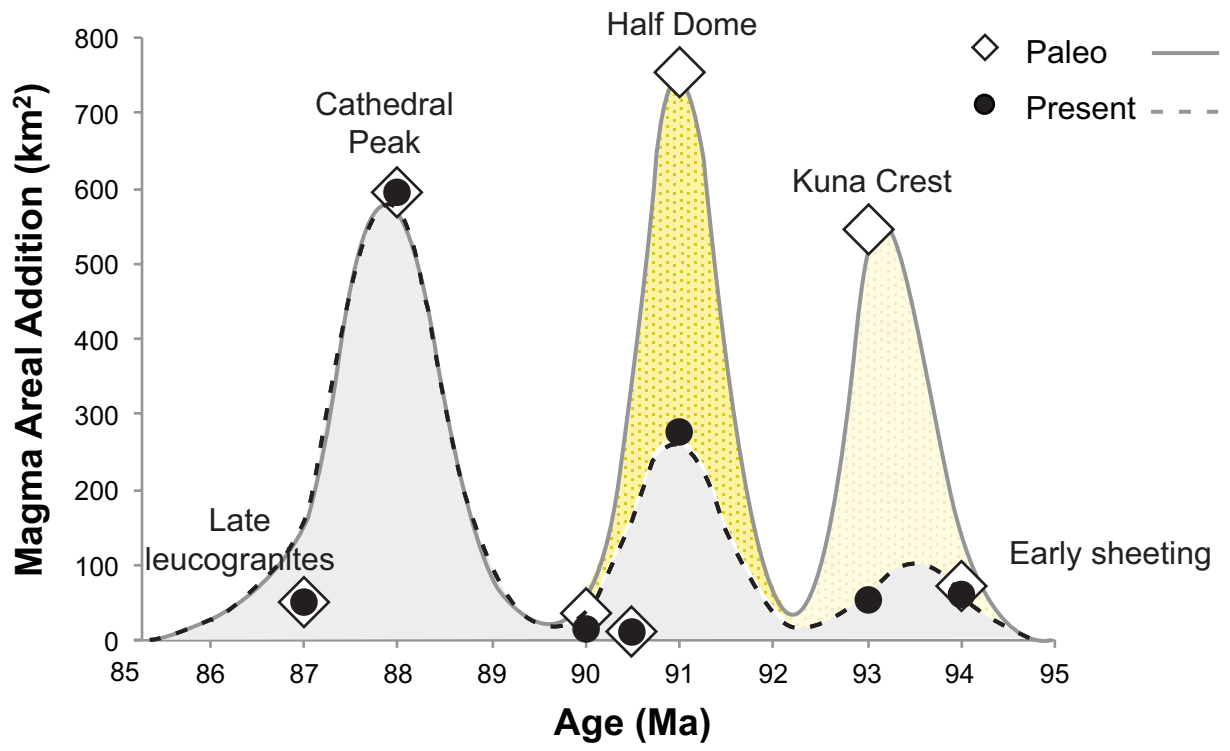


Figure 15



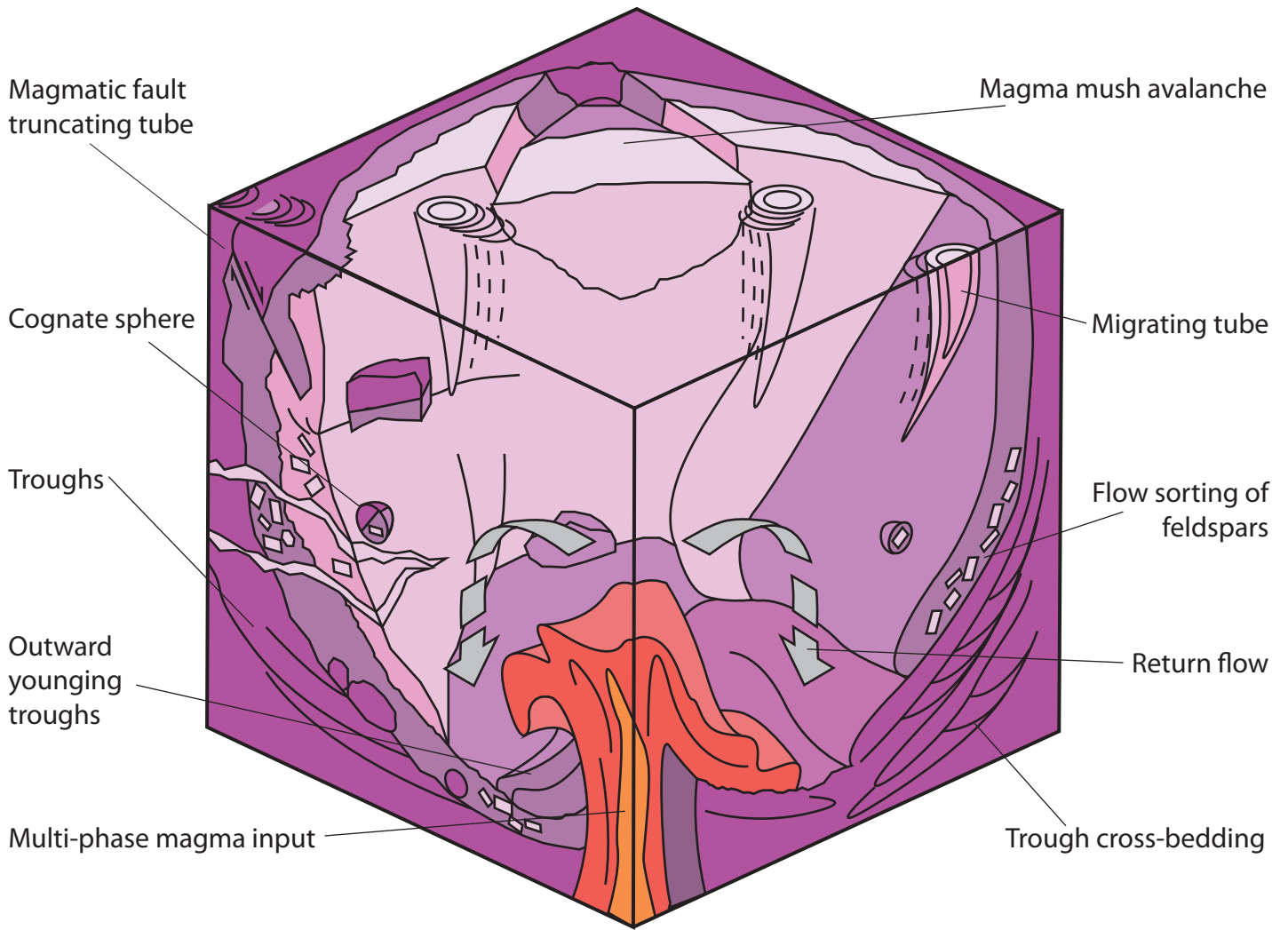


Figure 16